# TECHNICAL MEMORANDUM

## X-105

INVESTIGATION AT MACH NUMBERS OF 0.20 TO 3.50 OF A
BLENDED DIAMOND WING AND BODY COMBINATION OF
SONIC DESIGN BUT WITH LOW WAVE-DRAG
INCREASE WITH INCREASING
MACH NUMBER

By George H. Holdaway, Jack A. Mellenthin, and
Elaine W. Hatfield

Ames Research Center
Moffett Field, Calif.

Declassified September 1, 1961

**NATIONAL AERONAUTICS AND SPACE ADMINISTRATION**

**WASHINGTON**                                    October 1959

NATIONAL AERONAUTICS AND SPACE ADMINISTRATION

TECHNICAL MEMORANDUM X-105

# INVESTIGATION AT MACH NUMBERS OF 0.20 TO 3.50 OF A BLENDED DIAMOND WING AND BODY COMBINATION OF SONIC DESIGN BUT WITH LOW WAVE-DRAG INCREASE WITH INCREASING MACH NUMBER

By George H. Holdaway, Jack A. Mellenthin, and
Elaine W. Hatfield

## SUMMARY

A diamond wing and body combination was designed to have an area distribution which would result in near optimum zero-lift wave-drag coefficients at a Mach number of 1.00, and decreasing wave-drag coefficients with increasing Mach number up to near sonic leading-edge conditions for the wing. The airfoil sections were computed by varying their shapes along with the body radii (blending process) to match the selected area distribution and the given plan form. The exposed wing sections had an average maximum thickness of about 3 percent of the local chords, and the maximum thickness of the center-line chord was 5.49 percent. The wing had an aspect ratio of 2 and a leading-edge sweep of 45°. Test data were obtained throughout the Mach number range from 0.20 to 3.50 at Reynolds numbers based on the mean aerodynamic chord of roughly 6,000,000 to 9,000,000.

The zero-lift wave-drag coefficients of the diamond model satisfied the design objectives and were equal to the low values for the Mach number 1.00 equivalent body up to the limit of the transonic tests. From the peak drag coefficient near M = 1.00 there was a gradual decrease in wave-drag coefficient up to M = 1.20. Above sonic leading-edge conditions of the wing there was a rise in the wave-drag coefficient which was attributed in part to the body contouring as well as to the wing geometry.

The diamond model had good lift characteristics, in spite of the prediction from low-aspect-ratio theory that the rear half of the diamond wing would carry little lift. The experimental lift-curve slopes obtained at supersonic speeds were equal to or greater than the values predicted by linear theory. Similarly the other basic aerodynamic parameters, aerodynamic center position, and maximum lift-drag ratios were satisfactorily predicted at supersonic speeds.

INTRODUCTION

The design of airplanes is largely a matter of compromise. This is indicated by theoretical considerations of the selection of a wing plan form as reported in references 1, 2, and 3. For instance, the diamond wing which is the best structural shape of the zero-taper-ratio plan form is generally considered aerodynamically the poorest. Aerodynamicists point out on the basis of low-aspect-ratio or slender-body theories, that the rear half of a low-aspect-ratio diamond wing does not produce lift (ref. 1 or 4), and the zero sweep of the mid-chord line results in high transonic wave drag (refs. 1 through 5). For most low-aspect-ratio wing-body combinations, the wave drag at Mach number 1.00 can be reduced a large amount by the application of the simple area rule of reference 6; however, at Mach numbers only slightly above 1.00 the wave-drag coefficients will generally increase considerably (in particular for configurations with unswept wings). Similarly the supersonic area rule of reference 7 permits one to design for supersonic Mach numbers, but the procedures are more complicated and will result in an increase in wave-drag coefficients at nondesign Mach numbers. The area rules are usually applied by selecting a wing of fixed plan form and thickness distribution and shaping a fuselage to provide a smooth area distribution. A more flexible approach used in the present investigation was to vary both the wing thickness distribution and the fuselage shape to obtain a blended wing-body combination.

The purpose of the investigation was to seek the lowest possible wave drag at Mach number 1.00 (configuration made optimum at $M = 1.00$), which was consistent with a decreasing supersonic wave-drag coefficient. A brief statement of the design concept involved is to concentrate the wing volume near the body center line with a favorable or minimum distortion with Mach number of the area distributions defined by the theory of reference 7. Details of the concepts and procedures used in the design of the test model (aspect-ratio-2 diamond wing) are given in appendix B. The symbols used in the report (including appendix B) are listed in appendix A.

Experiments were conducted on the diamond wing-body combination at Mach numbers from 0.20 through 3.50 and at Reynolds numbers per foot that ranged from 1,000,000 to 6,000,000. Data were taken at each Mach number at a Reynolds number per foot of at least 3,000,000 to 4,000,000. The Reynolds numbers based on the mean aerodynamic chord of 26.67 inches would be, of course, over twice the numbers stated. Also tested at transonic speeds was a body with the same area distribution as the wing-body combination. As a check on the experimental results, theoretical predictions were made of the friction drag, zero-lift wave drag, drag due to lift, lift-curve slope, maximum lift-drag ratio, and aerodynamic center position of the wing-body combination.

## MODELS AND TESTS

The geometric details of the diamond wing and body combination are presented in figures 1 through 3 and in tables I and II. The radii for the body components are listed in table I. The forward and rearward body components are defined by the design area distribution, $KA_{25}$, shown in figure 2. The central portion of the body was designed to be as small as practical with sufficient space for the strain-gage balance which measured the aerodynamic forces. The low-drag shape selected for this central portion was part of a von Kármán ogive ($l$ = 40 in. and $r_b$ = 1.625 in.) defined by the following equation (also see table I):

$$ r = \frac{r_b}{\sqrt{\pi}} \sqrt{\cos^{-1}\frac{1-2x}{l} - \frac{1}{2}\sin 2\left(\cos^{-1}\frac{1-2x}{l}\right)} $$

and was a cylinder for the body stations rearward of 40 inches. Experimental wave-drag results and pressure distributions for a von Kármán ogive are reported in reference 8. The M = 1.00 equivalent body of the wing-body combination was also tested and is defined in table I and figure 1(b).

The wing coordinates are listed in table II. The wing-thickness distribution was computed as described in appendix B and is illustrated in figure 3. The wing thickness in each case is formed by straight-line elements perpendicular to the model center line forming triangular spanwise sections. Representative maximum thicknesses in percent chord are 5.49, 4.04, and 3.07 for center-line, body juncture (2 in. from the center line), and mean aerodynamic chords respectively. The average maximum thickness of the exposed wing was about the same as the maximum thickness of the mean aerodynamic chord.

Both the diamond model and its equivalent body were tested in the Ames 14-foot transonic wind tunnel at Mach numbers of 0.60 through 1.20. The diamond model was also tested in the Ames 12-foot subsonic pressurized wind tunnel and in the 9- by 7-foot and the 8- by 7-foot supersonic test sections of the Ames Unitary Plan wind tunnel. The latter supersonic facilities are described in reference 9. A photograph of the diamond model in the 8- by 7-foot supersonic test section is shown in figure 4. The equivalent body is shown in the perforated test section of the transonic tunnel in figure 5. The Mach number range of the tests in each facility as well as the range of the other test variables is shown in the following table:

| Wind tunnel throat | M | R/ft | $\alpha$, deg | Transition |
|---|---|---|---|---|
| 12-foot | 0.20 | 3,000,000 and | -4 to 26 | Free |
| 12-foot | 0.50 | 6,000,000 | -4 to 18 | Free |
| 14-foot | 0.60 to 0.80 | 3,500,000 to 4,000,000 | -2 to 11 | Free and fixed |
| 14-foot | 0.80 to 1.20 | 4,000,000 | -2 to 6 | Free and fixed |
| 9- by 7-foot | 1.55 | 4,000,000 | -2 to 7 | Fixed |
| 9- by 7-foot | 1.55 to 2.35 | 3,000,000 | -2 to 11 | Fixed |
| 8- by 7-foot | 2.50 to 3.00 | 3,000,000 and 4,000,000 | -2 to 12 | Free and fixed |
| 8- by 7-foot | 3.00 to 3.50 | 3,000,000 | -2 to 12 | Free and fixed |
| 8- by 7-foot | 2.50 to 3.50 | 1,000,000 | -2 to 12 | Free |

Three-component aerodynamic forces and moments were measured and corrected by standard procedures. For the model sizes and shapes, the force corrections for blockage and buoyancy were generally found to be negligible. Wall interference corrections were required for the angle of attack and drag data obtained in the subsonic wind tunnel, and these corrections were made based on the theory of reference 10. At all Mach numbers, the drag coefficients were adjusted by equating the body base pressures to free-stream static pressures. All aerodynamic coefficients are based on the complete plan-form area of the diamond wing of 800 square inches. The pitching-moment coefficients were computed about a longitudinal center 34.50 inches rearward of the nose of the body or 7.5 percent of the root chord forward of the centroid of the wing area. This position was selected for neutral longitudinal stability at supersonic speeds.

The procedures used to compute the friction drag and to fix transition, and the effects of the boundary-layer trip are discussed in appendix C; however, a brief description will be given here of the distributed roughness used to fix the location of the boundary-layer transition from laminar to turbulent flow. The grit size required (mean height of about 0.040 in.) was determined by preliminary tests at $M = 3.50$ and was used on the body and the wing at all Mach numbers although the size was excessive for the lower Mach numbers. A laminar-flow area of 5 percent of the wing area was allowed (i.e., the grit was located 1.13 in. rearward of the wing leading edge and of the body nose in a streamwise direction).

RESULTS AND DISCUSSION

The basic data are presented in figures 6 through 10. These figures illustrate that the effects of the Reynolds number changes were generally small; however, the Reynolds numbers will be noted where the effect on the drag data may be of some importance. The discussion will deal mainly with data taken at a Reynolds number per foot of 3,000,000 or 4,000,000. These basic data plots also indicate that the effect of fixing transition is relatively small and primarily effects the drag data. The effect of fixing transition is discussed in appendix C, so the following discussion is directed toward transition-fixed results.

The discussion is presented in two parts: the first section is an analysis of the zero-lift wave drag (the major design parameter), and the second is an analysis of the aerodynamic trends with Mach number.

Zero-Lift Wave Drag

A fundamental way of experimentally evaluating how well the diamond model met the design objective (to seek a low wave drag at Mach number 1.00, which was consistent with a decreasing supersonic wave-drag coefficient) is to compare its wave drag with that of its equivalent body which is in turn compared with an optimum body. It should be remembered that the wave drag of a wing-body combination is usually greater than that for its M = 1.00 equivalent body at Mach numbers only slightly above 1.00. Only transonic data were obtained for the equivalent body and thus the comparisons are made at these speeds. At transonic speeds the diamond model fully met the design expectations as shown by the wave-drag coefficients in figure 11. Essentially identical zero-lift wave-drag coefficients were obtained for the diamond model and its equivalent body at Mach numbers up to 1.20. From the peak drag coefficient near M = 1.00 there was a gradual decrease in drag coefficient up to M = 1.20.

In figure 12 the wave-drag coefficients of the equivalent body are compared with those for a minimum wave-drag body and with theoretical predictions based on the method of reference 11. The data points are shown for direct evaluation. The coefficients are based on the plan-form area of the diamond wing. Each body had a closed-body fineness ratio of 12.5 and the body shapes are discussed fully in appendix B. The data for the Sears-Haack body (minimum transonic wave-drag body for prescribed volume and length, ref. 12) were obtained from the investigation of reference 13. Both bodies had transition fixed; however, the grit used on the Sears-Haack body was selected for transonic speeds and was much smaller (about 0.003 in. in diameter). Note that the wave-drag coefficients for the equivalent body are substantiated by theory and are as low as or lower than the minimum wave-drag body for Mach numbers greater

6

than 1.04. The difference in wave-drag coefficients at M = 1.00 between
the bodies is much greater than that indicated by theory (see appendix B)
and may be partially due to the difference in the size of the grit used
to fix transition.

The diamond model was designed for M = 1.00 and one would not
expect the wave-drag coefficients to continue to decrease through Mach
numbers at which the velocities normal to the wing leading edge are sonic
or supersonic. It is of interest to see how experiment and predictions
would compare at higher supersonic Mach numbers. Such comparisons are
made in figure 13, with theoretical predictions based on 49 harmonics
representing the derivatives of the area curves. Predictions were also
made with 25 harmonics; however, the larger number of terms was required
to give a good representation of the area distributions. At transonic
speeds the solutions for the diamond model based on 25 harmonics were
satisfactory and almost equal to the 49-term solution.

The theoretical computations of wave drag were made by two methods,
each of which was based on the procedures of reference 11. Each method
would give essentially the same answer if the body alone equivalent area
distribution did not vary with Mach number (i.e., slender bodies accept-
able to the theory (ref. 7)). Thus at the higher supersonic Mach numbers
where different answers were obtained as shown in figure 13, both theo-
retical predictions are questionable. It is of interest to note that
this fact plus an analysis of the area distributions indicate that the
rise in wave-drag coefficients at Mach numbers near sonic leading-edge .
conditions of the wing may be attributed in part to the body contouring.
Method 1, used for the results presented in figure 13, is the more
convenient of the two methods, and it involves the use of various combi-
nations of equivalent area distributions obtained from oblique cuts of
the total wing-body combination as a function of roll angle $\theta$. It is
theoretically more correct to handle the variation of the body area
independently of the wing area, because for a body of revolution the area
distribution varies only with Mach number and not with roll angle $\theta$.
This latter procedure was used for the results listed in figure 13 as
method 2. Experimental data were not available at sonic-leading-edge
conditions; however, it is evident that both theoretical methods tend to
overestimate the wave drag under these circumstances. Note in figure 13
that at a Mach number of 3.00 the higher Reynolds number data agree better
with the theory. The results of method 1 agree better with the experi-
mental results at the higher supersonic speeds, so these theoretical
results were used in determining the theoretical lift-drag ratios presented
in the next section of the report.

Aerodynamic Trends With Mach Number

Presented in figure 14 are summary plots of experimental and theoretical values of drag due to lift, aerodynamic-center location, lift-curve slope, and maximum lift-drag ratios for the diamond model. At supersonic speeds the lift-curve slope and the aerodynamic-center position were computed with equations of linearized theory available in reference 1 or 14. The theoretical results at subsonic speeds were computed from the curves of reference 15 which is based on a simplified lifting-surface theory. The theory at $M = 1.00$ is based on low-aspect-ratio theory (ref. 1 or 4) and is directly applicable only to delta wings. Except for the zero-lift drag data, all the theoretical results are for the wings alone without thickness. The friction drag was computed as outlined in appendix D and the wave drag at zero lift was computed by method 1 as discussed previously. The maximum lift-drag ratios were predicted from a combination of these results.

The theoretical drag due to lift parameter $C_{D_i}/C_L^2$, as shown in figure 14(a), was computed as the reciprocal of the theoretical lift-curve slope at all Mach numbers and therefore was without leading-edge thrust. Also shown in figure 14(a) is the value, $C_{D_i}/C_L^2 = 1/\pi A$, for minimum vortex drag due to lift. The results indicate that the sharp-edged diamond model did have some leading-edge thrust at subsonic and transonic Mach numbers; however, for Mach numbers greater than 2.50 the experimental drag due to lift parameters approached the theory without leading-edge thrust, and theory and experiment were in good agreement. The subsonic tests were without the transition fixed, but the laminar-flow region for the low-speed tests should be comparable to the 5 percent allowed (1.13 in. streamwise).

The variation in aerodynamic-center position with Mach number occurred primarily at transonic speeds as shown in figure 14(b). The subsonic and supersonic levels were reasonably well predicted, although the theoretical shift in aerodynamic-center position was less than that obtained experimentally.

Probably the most interesting result of this investigation is the good lift characteristics of the diamond plan form, in spite of the prediction that the rear half of the wing would carry little lift according to low-aspect-ratio theory. At $M = 1.00$ the experimental lift-curve slope (fig. 14(d)) for the diamond model (0.0596) was higher than the theoretical value for a similar aspect-ratio-2 delta wing (0.0548). Similarly, for Mach numbers equal to 1.55 or greater (where data were available) the experimental lift-curve slopes were equal to or greater than the values predicted by linear theory (see fig. 14(d)).

The maximum lift-drag ratios of figure 14(c) reflect the previously discussed zero-lift wave-drag coefficients, the drag due to lift, and the lift-curve slopes. The excellent transonic zero-lift wave-drag coefficients, some leading-edge thrust, and high lift-curve slopes all helped to produce high maximum lift-drag ratios of 9.5 or better at transonic speeds. At the higher supersonic speeds the agreement between theory and experiment is very good, but probably would be improved even further for a thinner wing and a body with less contouring.

## CONCLUDING REMARKS

The zero-lift wave-drag coefficients of the diamond model were essentially identical with the low values for its $M = 1.00$ equivalent body up to the limit of the transonic tests $(M = 1.20)$. From the peak wave-drag coefficient near $M = 1.00$ there was a gradual decrease in wave-drag coefficient up to $M = 1.20$. Near sonic leading-edge conditions of the wing there was a rise in the wave-drag coefficient which was attributed in part to the body contouring but was primarily attributed to the wing geometry.

The diamond model had good lift characteristics, in spite of the possibility that the rear half of the diamond wing would carry little lift according to low-aspect-ratio theory. The experimental lift-curve slopes obtained at supersonic speeds were equal to or greater than the values predicted by linear theory. Similarly the aerodynamic center position, and the maximum lift-drag ratios were satisfactorily predicted at supersonic speeds.

Ames Research Center
National Aeronautics and Space Administration
Moffett Field, Calif., July 8, 1959

APPENDIX A

SYMBOLS

A   aspect ratio

$A_N$   area distribution of the approximate Newtonian nose shape

$A_n$   coefficients determining the magnitude of the harmonics of a Fourier sine series

$\dfrac{b}{2}$   semispan

$C_D$   drag coefficient
(All aerodynamic coefficients are based on the total wing area.)

$\dfrac{C_{D_i}}{C_L^2}$   slope of the curve of drag coefficient due to lift vs. lift coefficient squared, taken at the lift coefficient data point nearest to that for $\left(\dfrac{L}{D}\right)_{max}$

$C_{D_o}$   zero-lift drag coefficient

$C_L$   lift coefficient

$C_{L_\alpha}$   lift-curve slope, per deg

$C_m$   pitching-moment coefficient about body station 34.50 measured from the body nose

$c_R$   center line, or wing-root chord

$\bar{c}$   mean aerodynamic chord

$E'(m)$   complete elliptic integral of the second kind

$k$   average height of transition grit

$KA_{25}$   M = 1.00 equivalent body radii or area distribution

$\left(\dfrac{L}{D}\right)_{max}$   maximum lift-drag ratio

$l$   model length

M           Mach number

m           $\beta \cot \Lambda$

N           total number of terms used in computing $\Delta C_{D_O}$

n           specific term or harmonic used to define an area distribution

R           Reynolds number

r           body radius

$r_O$         body maximum radius

$r_b$         body base radius

S           cross-sectional area

$S_W$         total wing area

$\dfrac{t}{2}$         wing semithickness

x           body station, measured aft from model nose

$\dfrac{x_1}{c_R}$        aerodynamic center location, where $x_1$ = station measured from leading edge of wing-root chord

V           volume

$\dfrac{V}{V_{A_2}}$        volume relative to a Sears-Haack body with minimum wave drag for given volume and length (ref. 12)

$\alpha$           angle of attack

$\beta$           $\sqrt{M^2 - 1}$

$\Delta C_{D_O}$         zero-lift wave-drag coefficient

$\theta$           roll angle of a cutting plane tangent to a Mach cone as measured between the z axis and the intersection of the cutting plane with the yz plane

$\Lambda$           angle of sweepback of leading edge of wing

$\xi$           $\dfrac{\text{cotangent of sweep angle of plan-form leading edge}}{\text{cotangent of sweep angle of plan-form trailing edge}}$

$\varphi$           transformation of the length x to radians, $\cos^{-1}\dfrac{2x - 1}{l}$
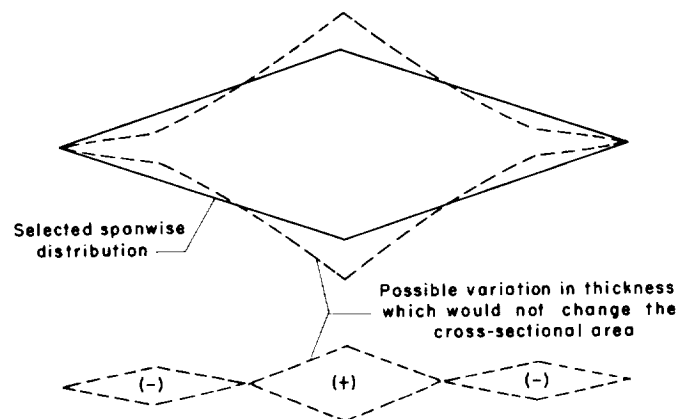
APPENDIX B


DESIGN PROCEDURE


As mentioned in the introduction to this report, the general approach was to seek the lowest possible wave drag at Mach number 1.00 which was consistent with a decreasing supersonic wave-drag coefficient. The basic design concept was to concentrate the wing volume near the body center line with a favorable or minimum distortion of a selected area distribution with changes in Mach number. The distortions in the area distributions are the result of obtaining equivalent area distributions from oblique cuts tangent to the Mach cone according to the theory of reference 7.

The diamond plan form selected was not considered as ideal from a wave-drag standpoint, but rather as a probable shape of interest to airplane designers. However, by selecting a plan form with zero taper ratio, the wing volume would naturally tend to be concentrated near the body center line. The symmetry of the diamond plan form justified its selection, because the distortions of its area curves could also be made symmetrical.

With the plan form specified the next step was to select a spanwise thickness distribution. The thickness distribution selected was formed by straight-line elements forming triangular spanwise sections (prependicular to the model center line), which incidently results in a rigid structural shape. Various cusp shapes were also considered which would further concentrate the wing volume along the model center line or improve the supersonic wave drag. Along this line of reasoning an idea of R. T. Jones is simply illustrated in sketch (a), where it is shown that the



Selected spanwise distribution

Possible variation in thickness which would not change the cross-sectional area

(-)   (+)   (-)

Sketch (a)

spanwise thickness distribution can be altered for some higher design
Mach number by adding zero area to the $M = 1.00$ area distribution. This
idea was not investigated very fully, but an application with parabolic
arcs, rather than the straight lines shown in sketch (a), was tried for
the diamond plan form for Mach numbers up to 1.20. Little improvement in
computed wave drag was indicated over the straight-line thickness distri-
bution; so these more complex distributions were not justified for the
conditions considered. For higher Mach numbers or for other configu-
rations, complex spanwise thickness distributions might be justified.
Other interesting types of wing thickness distributions formed by straight
lines are discussed in reference 16.

The area distribution was next selected to help compensate for the
distortion of the wing area distribution with Mach number. The area
distribution was also selected to have an equivalent body with near opti-
mum theoretical zero-lift wave drag. The area curves considered in the
selection of the design area distribution are shown in figure 15. The
length and the maximum cross-sectional area were held constant, although
a reduction in volume was allowed relative to the Sears-Haack body (mini-
mum transonic wave-drag body for given volume and length, ref. 12). The
area-distribution curve for this Sears-Haack body is shown in the lower
left-hand corner of figure 15, and the volume ratio is of course equal to
1.00. The derivative of this area curve is completely defined by the
amplitude of the second harmonic of a Fourier sine series. It may be
noted that all the other bodies had a reduction in volume and generally
an increase in drag. A reduction in zero-lift wave-drag coefficient was
computed for one area curve, defined by two terms of a sine series, shown
in the upper right-hand corner of figure 15. The upper left-hand curve
is that for a three-quarter power body, an approximation of the Newtonian
nose shape (based on impact theory, ref. 17), reflected to form a closed
body. The theoretical zero-lift wave-drag coefficients are quite similar
considering that the one area curve requires almost an infinite number of
terms ($N = 25$ for $\Delta C_{D_O}$ shown) for definition while the other curves
required only one or two terms. The coefficients are based on a wing
area of 800 square inches.

A preliminary analysis of these area distributions with the diamond
plan form was made to indicate how the theoretical wave-drag coefficients
would vary with $\beta \cos \theta$ or roughly Mach number as follows:

| Plan form | Area distribution (see fig. 15) | | | | Drag coefficient, $\Delta C_{D_o}$ (N = 25) | | |
|---|---|---|---|---|---|---|---|
| | $A_2$ | $A_3$ | $A_4$ | $A_{n>4}$ | $\beta \cos \theta = 0$ | $\beta \cos \theta = 0.6633$ | $\beta \cos \theta = 3.3541$ |
| Diamond | $A_N$ | $A_N$ | $A_N$ | $A_N$ | 0.0034 | 0.0023 | 0.0040 |
| Diamond | 1.696[1] | 0 | 0 | 0 | .0025 | .0059 | |
| Diamond | 1.405 | 0 | -.727 | 0 | .0026 | .0053 | |
| Diamond | 1.551 | 0 | -.360 | 0 | .0023 | .0053 | |

[1]Sears-Haack body, minimum wave drag for given volume and length from linearized theory. See reference 12.

The $\beta \cos \theta$ value of 0.6633 represents the maximum cutting angle for M = 1.20 and the value of $\beta \cos \theta$ = 0 represents all cutting angles for M = 1.00. From these data it was indicated that the $A_N$ area distribution with the diamond wing fully met the desired design objectives, because the wave-drag coefficient is near optimum at M = 1.00 and decreases with increased Mach number up to 1.20. For the highest value of $\beta \cos \theta$ (3.3541) the theory was not relied upon for the preliminary analysis, since the velocity components normal to the wing leading edge were supersonic, however, the indicated wave-drag coefficient was reasonably low. Thus it was decided to use the ($A_N$) area distribution; however, some modifications to the selected area distribution were made, as shown in figure 16. To be consistent with the drag coefficients shown in table V, the $A_N$ distribution was replaced by the distribution defined by 25 harmonics ($A_{25}$). Next the maximum cross-sectional area was corrected to the original value (to maintain a fixed maximum cross-sectional area) as shown in figure 16 to result in the $KA_{25}$ area distribution which was the design area curve used. This area distribution was cut off at station 60, with a curve with zero slope at the base and defined by 25 harmonics, to permit sting-mounting of the models. These modifications to the design area curve resulted in only a small change in the computed wave-drag coefficient from the original value of 0.0034 to 0.00366 and 0.00369 for N = 25 and N = 49, respectively.

With the area distribution and the wing spanwise thickness distribution specified (triangular spanwise sections) the wing section could be computed directly if the model was a wing alone configuration. For the present investigation, forward and rearward body components were required because the selected length of the area curve was greater than the wing streamwise length. Also a minimum body size was specified in the central region of the model to permit installation of the strain-gage balance. For an actual airplane, similar body components would be a function of the engine size or cockpit size. Temporarily ignoring the minimum body, the next step in the model design was to compute the thickness distribution of the wing along the model center line as shown in sketch(b).

Body station x
Sketch (b)
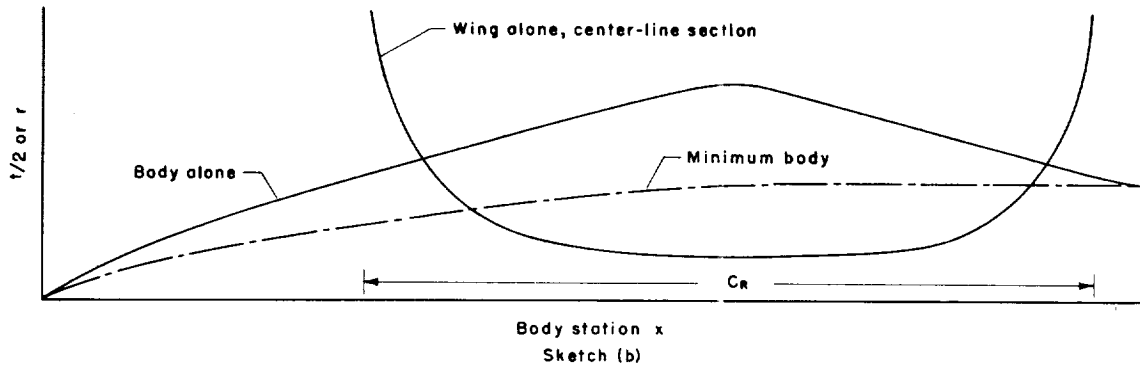
The wing thickness at the leading and trailing edges of the root chord
approached infinity as the span approached zero. In the region where the
minimum body radii were greater than half the wing thickness, the combined
area distribution would be greater than that specified and thus the exposed
minimum-body area was removed from the given area distribution and the
wing thickness was recomputed. The convergence was rapid because of the
small size of the exposed minimum-body area. The blending process was the
last step in the design. The root section of the wing was made to have
zero thickness at the leading and trailing edges, and the thickness of
the wing and the radii of the body were varied or blended as shown in
sketch (c) to match the given area curve and to avoid abrupt changes in



Body station, x
Sketch (c)
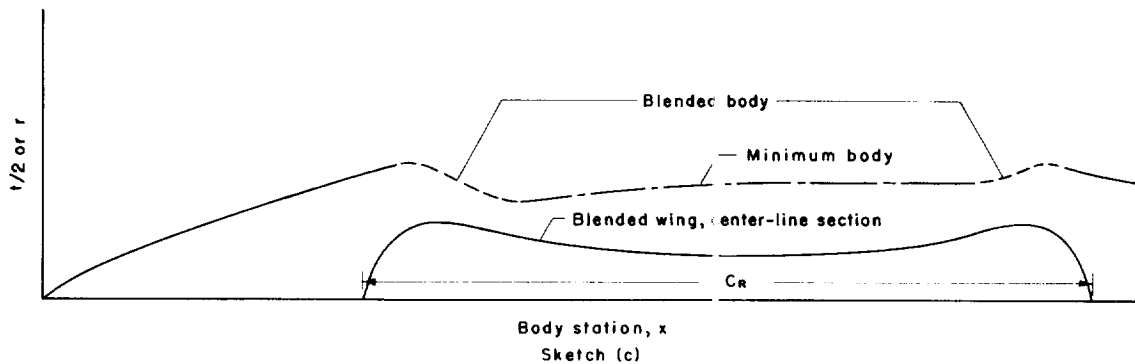
surface slope in the wing or the body components. The body blending of
course did not occur unless the wing extended outside the body. The
center line or root airfoil sections had the greater surface slopes and
the outboard sections were almost biconvex as may be seen in figure 1 and
interpreted from figure 3. The blended regions of the final body are
also noted in table I.

APPENDIX C

FIXING BOUNDARY-LAYER TRANSITION AND FRICTION DRAG

Confidence in the results of a zero-lift wave-drag investigation can be obtained only if the variations in friction-drag coefficients with Mach number are known or may be computed accurately. This is because the experimental wave drag is determined by subtracting the estimated friction drag from the measured zero-lift drag. The laminar and turbulent friction drag were computed at $M = 0$ with zero heat transfer by the method of reference 18. The variation of the friction-drag coefficients with Mach number was computed from the following equations:

Laminar flow, reference 19

$$\frac{c_{D_f}\sqrt{R}}{(c_{D_f}\sqrt{R})_{M=0}} = \left(1 + 0.6 \; \frac{\gamma-1}{2} \; M^2\right)^{-0.12} \tag{1}$$

Turbulent flow (smooth surface), reference 20

$$\frac{c_{D_f}}{\left(c_{D_f}\right)_{M=0}} = \left(1 + \frac{\gamma-1}{2} \; M^2\right)^{-0.467} \tag{2}$$

Turbulent flow (rough surface), reference 21

$$\frac{c_{D_f}}{\left(c_{D_f}\right)_{M=0}} = \left(1 + r \; \frac{\gamma-1}{2} \; M^2\right)^{-1} \tag{3}$$

where the recovery factor, $r = 0.86$ and $\gamma = 1.4$. This latter equation is required for the wing area covered by a distributed roughness.

Because the extent of the laminar boundary-layer flow will vary with Reynolds number and Mach number, a rigorous wave-drag comparison between models can be obtained only if identical regions of laminar, turbulent, and turbulent-rough flow are maintained at each test condition. Fixing transition at high Mach numbers and low Reynolds numbers on wings is

16

difficult as indicated in reference 22. The single-element roughness used in reference 22 resulted in large drag (considered to be primarily wave drag) and was not adequate in fixing transition at M = 3.53 and Reynolds numbers per foot of approximately 1,400,000 to 2,700,000. This appendix described what was done to fix transition on the diamond model at M = 3.50 and R per foot = 3,000,000, and what effect fixing transition had on the aerodynamic data.

## SELECTION OF DISTRIBUTED ROUGHNESS

Prior experience rejected single-element roughness for the boundary-layer trip and suggested the use of a distributed roughness. Based on estimates of the short length of the laminar-flow at subsonic speeds at R per foot = 4,000,000 the following grit location and extent was selected. The distributed roughness was formed by first spraying a thin coat of cement and then spraying (at low pressure) the grit on a strip of the wing 0.22 inch wide and 1.13 inches rearward of the wing leading edge and the body nose (measured in a streamwise direction). This resulted in fixing the laminar region to 5 percent of the wing area and the rough region to 1 percent of the wing area. Grit concentration was approximately 200 per square inch and this value was used in the computation of friction drag. The size of the grit was determined from preliminary tests in the 8- by 7-foot supersonic wind tunnel. The end of the laminar-flow region was determined by the use of fluorine sublimation material as discussed in reference 23. The grit finally selected had a mean height of 0.040 inch and varied from about 0.030 to 0.050 inch. The grit location on the wing and the grit size is indicated in the full-scale photograph of figure 17. In figure 17 the painted white lines are located 3 inches apart in the streamwise direction. Laminar flow is indicated ahead of the grit, mixed vortex and laminar flow are indicated by the parallel streaks, and fully turbulent flow is indicated where the expanding black streaks coalesce. In this preliminary test the grit was not placed close enough together in a couple of regions as indicated by the extended white streaks representing localized regions of laminar flow. More uniform grit spacing was used when the force data were obtained.

An example where transition was not considered to be fixed is shown in figure 18(a) for a Reynolds number per foot of 1,000,000 (the white fluorine crystals were not removed from the wing tip). The satisfactory performance of the 0.040-inch grit at R per foot = 3,000,000 and M = 3.50 is shown for comparison in figure 18(b). The grit was sufficiently large that it extended out of the boundary layer; however, if the grit were located further rearward, the length of the laminar-flow region would be increased at high supersonic Mach numbers and would be decreased at subsonic Mach numbers. Smaller sized grit in the same location, of a size to lie within the boundary layer, did not fix transition. These results indicate a need for further investigation of the parameters used

in the suggested roughness Reynolds numbers recommended in references 24, 25, and 26. In particular the use of the curves of reference 26 for Mach numbers of the order of 3.00 or greater does not apparently apply for cases such as the present investigation where transition is desired near the wing leading edge. The roughness Reynolds number for the case of figure 18(b) is about 7,000 or 5 to 7 times greater than that indicated by the curves of reference 26 for two-dimensional and three-dimensional flow, respectively. Perhaps the velocity and temperature used in the roughness Reynolds number should be based on other boundary-layer parameters such as the momentum or displacement thickness which would better group the results for roughness particles both within and partially outside the boundary layer. The sublimation procedure used in the present investigation to indicate transition (with the criteria that there should be no laminar flow of consequence rearward of the grit) is probably more conservative than the detection of spots of turbulence used in references 24, 25, and 26.

## EFFECT ON THE AERODYNAMIC DATA

Previously presented data of figure 7 indicated that fixing transition had very little effect on the lift or moment data and the greatest effect on the zero-lift drag coefficients. A summary plot of the zero-lift drag coefficients for the diamond model is presented in figure 19.

The addition of the distributed roughness increased the zero-lift drag coefficients at the higher supersonic Mach numbers to a lesser degree than at subsonic Mach numbers ($\Delta C_{D_O}$ = 0.0013 to 0.0017, respectively). Also the experimental increase in zero-lift drag is very nearly the same as the computed increase in friction drag (note, in particular, the higher Reynolds number data at M = 3.00). These two facts qualitatively indicate that the grit did not produce wave drag in spite of its large size. The increase in drag due to fixing transition with the grit was a reasonable amount and was estimated quite well as shown in figure 19. With transition free tests, the line of transition between laminar and turbulent flow as indicated by the sublimation material was quite irregular at subsonic speeds so the uncertainty in predicting the laminar region is indicated by the shaded region. The base-drag coefficients which were typical of all bodies tested with or without wings are included in this figure for completeness of all drag components involved at zero lift, and illustrate that the body base may contribute to the zero-lift drag if the base is not completely filled with jet exhaust.

Since the effect of fixing transition was not very large on the zero-lift drag coefficients, the effect on the maximum lift-drag ratios was not large as shown in figure 20. The greatest reduction in $(L/D)_{max}$ was about 0.8 at subsonic speeds, and only 0.2 to 0.4 at supersonic speeds.
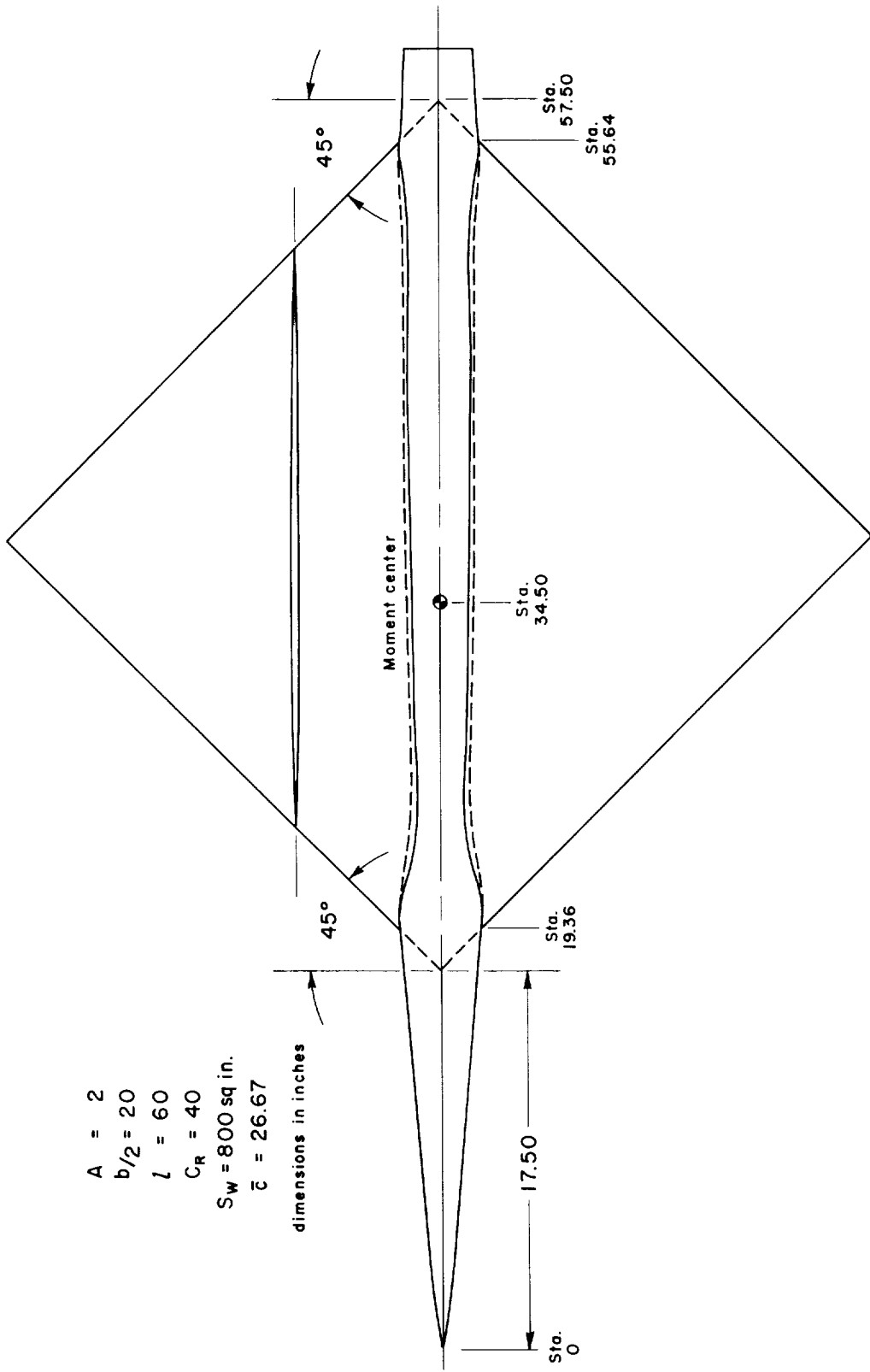
REFERENCES

1. Donovan, A. F., and Lawrence, H. R.: Aerodynamic Components of Air-craft at High Speeds. Princeton Univ. Press, 1957. (High Speed Aerodynamics and Jet Propulsion, vol. VII, pp. 100, 197-226)

2. Snow, R. M., and Bonney, E. A.: Aerodynamic Characteristics of Wings at Supersonic Speeds. Bumblebee Series Rep. 55, Johns Hopkins Univ. Appl. Phys. Lab., Mar. 1947.

3. Bishop, R. A., and Love, E. G.: Charts of the Theoretical Wave Drag of Wings at Zero Lift. British R.A.E. TN Aero 2421, June 1956.

4. Jones, Robert T.: Properties of Low-Aspect-Ratio Pointed Wings at Speeds Below and Above the Speed of Sound. NACA Rep. 835, 1946. (Supersedes NACA TN 1032)

5. Robinson, A.: The Wave Drag of Diamond-Shaped Airfoils at Zero Incidence. British R.A.E. TN Aero 1784, A.R.C. 9780, R. & M. 2394, 1946.

6. Whitcomb, Richard T.: A Study of the Zero-Lift Drag-Rise Charac-teristics of Wing-Body Combinations Near the Speed of Sound. NACA Rep. 1273, 1956. (Supersedes NACA RM L52H08)

7. Jones, Robert T.: Theory of Wing-Body Drag at Supersonic Speeds. NACA Rep. 1284, 1956. (Supersedes NACA RM A53H18a)

8. Jorgensen, Leland H.: Correlation by the Hypersonic Similarity Rule of Pressure Distributions and Wave Drags for Minimum-Drag Nose Shapes at Zero Angle of Attack. NACA RM A53F12, 1953.

9. Huntsberger, Ralph F., and Parsons, John F.: The Design of Large High-Speed Wind Tunnels. AGARD Rep. AG15/P6, May 4, 1954.

10. Glauert, H.: The Elements of Aerofoil and Airscrew Theory. Cambridge Univ. Press, 1937.

11. Holdaway, George H., and Mersman, William A.: Application of Tchebichef Form of Harmonic Analysis to the Calculation of Zero-Lift Wave Drag of Wing-Body-Tail Combinations. NACA RM A55J28, 1956.

12. Sears, William R.: On Projectiles of Minimum Wave Drag. Quart. Appl. Math., vol. IV, no. 4, Jan. 1947, pp. 361-366.

13. Holdaway, George H., Wallace, Minor R., Jr., and Hatfield, Elaine W.: A Transonic Investigation of the Effects of Semisubmerged-Store Cavities and of Slots on the Zero-Lift Drag of a Body of Revolution. NACA RM A57H19a, 1957.

14. Puckett, A. E., and Stewart, H. J.: Aerodynamic Performance of Delta Wings at Supersonic Speeds. Jour. Aero. Sci., vol. 14, no. 10, Oct. 1947, pp. 567-578.

15. De Young, John, and Harper, Charles W.: Theoretical Symmetric Span Loading at Subsonic Speeds for Wings Having Arbitrary Plan Form. NACA Rep. 921, 1950.

16. Peckham, D.: The Geometry of Wing Surfaces Generated by Straight Lines and With a High Rate of Thickness Taper at the Root. R.A.E. TN Aero 2451, May 1957.

17. Eggers, A. J., Jr., Resnikoff, Meyer M., and Dennis, David H.: Bodies of Revolution Having Minimum Drag at High Supersonic Airspeeds. NACA Rep. 1306, 1957.

18. Hall, Charles F., and Fitzgerald, Fred F.: An Approximate Method for Calculating the Effects of Surface Roughness on the Drag of an Airplane. NACA RM A7B24, 1947.

19. Rubesin, M. W., and Johnson, H. A.: A Critical Review of Skin-Friction and Heat-Transfer Solutions of the Laminar Boundary Layer of a Flat Plate. Trans. ASME, vol. 71, no. 4, May 1949, pp. 383-388.

20. Rubesin, Morris W., Maydew, Randall C., and Varga, Steven A.: An Analytical and Experimental Investigation of the Skin Friction of the Turbulent Boundary Layer on a Flat Plate at Supersonic Speeds. NACA TN 2305, 1951

21. Goddard, Frank E., Jr.: Effect of Uniformly Distributed Roughness on Turbulent Skin-Friction Drag at Supersonic Speeds. CIT Rep. 20-113, Sept. 1957.

22. Hopkins, Edward J., Keating, Stephen J., Jr., and Muhl, Richard R.: Forces and Pitching Moments on an Aspect-Ratio-3.1 Wing-Body Combination at Mach Numbers From 2.5 to 3.5 and Sublimation Studies of the Effect of Single-Element Roughness on the Boundary-Layer Flow. NACA RM A58E21a, 1958.

23. Main-Smith, J. D.: Chemical Solids as Diffusible Coating Films for Visual Indications of Boundary-Layer Transition in Air and Water. British R. & M. 2755, 1950. (Brit. R.A.E. Chem. 466, Feb. 1950)

24. Von Doenhoff, Albert E., and Horton, Elmer A.:   A Low-Speed Experimental Investigation of the Effect of a Sandpaper Type of Roughness on Boundary-Layer Transition.   NACA TN 3858, 1956.

25. Braslow, Albert L.:   Effect of Distributed Granular-Type Roughness on Boundary-Layer Transition at Supersonic Speeds With and Without Surface Cooling.   NACA RM L58A17, 1958.

26. Braslow, Albert L., and Know, Eugene C.:   Simplified Method for Determination of Critical Height of Distributed Roughness Particles for Boundary-Layer Transition at Mach Numbers of 0 to 5.   NACA TN 4427, 1958.

# TABLE I.- COORDINATES FOR BODIES, INCHES

| M = 1.00 equivalent body KA25 | | Diamond model | | M = 1.00 equivalent body KA25 | | Diamond model | |
|---|---|---|---|---|---|---|---|
| x | r | x | r | x | r | x | r |
| 0 | 0 | KA25 body | | 32.625 | 2.765 | 34.400 Von Karman | 1.554 |
| .375 | .075 | | | 33.375 | 2.820 | 35.200 ogive | 1.569 |
| .750 | .148 | | | 34.125 | 2.873 | 36.000 | 1.582 |
| 1.500 | .258 | | | 35.625 | 2.957 | 36.800 | 1.594 |
| 2.250 | .356 | | | 36.375 | 2.984 | 37.600 | 1.605 |
| 3.000 | .449 | | | 37.500 | 3.000 | 38.400 | 1.614 |
| 3.750 | .542 | | | 38.625 | 2.984 | 39.200 | 1.621 |
| 4.500 | .623 | | | 39.375 | 2.957 | 40.000 | 1.625 |
| 5.250 | .693 | | | 40.125 | 2.919 | Cylinder | |
| 6.000 | .761 | | | 41.625 | 2.820 | | |
| 6.750 | .830 | | | 42.375 | 2.765 | | |
| 7.500 | .903 | | | 43.125 | 2.709 | | |
| 8.250 | .976 | | | 44.625 | 2.603 | | |
| 9.000 | 1.048 | | | 45.375 | 2.555 | | |
| 9.750 | 1.116 | | | 46.125 | 2.509 | | |
| 10.500 | 1.179 | | | 46.875 | 2.464 | | |
| 11.250 | 1.238 | | | 47.625 | 2.420 | | |
| 12.000 | 1.296 | | | 48.000 | 2.400 | | |
| 12.750 | 1.353 | | | 48.375 | 2.374 | | |
| 13.125 | 1.388 | | | 49.125 | 2.326 | | |
| 13.875 | 1.448 | | | 49.875 | 2.275 | | |
| 14.625 | 1.509 | | | 50.625 | 2.221 | | |
| 15.375 | 1.570 | | | 51.375 | 2.166 | 51.000 | 1.625 |
| 16.125 | 1.630 | | | 52.125 | 2.110 | 52.000 Blended | 1.657 |
| 16.875 | 1.688 | | | 52.875 | 2.054 | 53.000 body | 1.730 |
| 17.500 | 1.733 | | | 53.625 | 2.000 | 54.000 | 1.827 |
| 18.000 | 1.762 | | | 54.375 | 1.948 | 55.000 | 1.878 |
| 19.000 | 1.823 | 19.360 | 1.860 | 55.125 | 1.896 | 55.640 | 1.860 |
| 19.875 | 1.896 | 20.000 Blended | 1.874 | 55.875 | 1.846 | KA25 body | |
| 20.625 | 1.948 | 21.000 body | 1.825 | 56.625 | 1.795 | | |
| 21.375 | 2.000 | 22.000 | 1.712 | 57.300 | 1.747 | | |
| 22.125 | 2.054 | 24.000 | 1.471 | 57.600 | 1.728 | | |
| 23.625 | 2.166 | 24.800 | 1.392 | 57.900 | 1.709 | | |
| 24.375 | 2.221 | 26.000 | 1.347 | 58.200 | 1.692 | | |
| 25.125 | 2.275 | 26.400 Von Karman | 1.360 | 58.500 | 1.677 | | |
| 26.625 | 2.374 | 28.000 ogive | 1.405 | 58.800 | 1.662 | | |
| 27.375 | 2.420 | 29.600 | 1.447 | 59.100 | 1.649 | | |
| 28.125 | 2.464 | 31.200 | 1.487 | 59.400 | 1.637 | | |
| 29.625 | 2.555 | 32.800 | 1.522 | 59.700 | 1.629 | | |
| 30.375 | 2.603 | 33.600 | 1.539 | 60.000 | 1.625 | | |
| 31.125 | 2.655 | | | | | | |

## TABLE II.- COORDINATES FOR DIAMOND WING, INCHES

| x \ y | 0 | 2.000 | 4.000 | 6.667 | 8.000 | 12.000 | 13.333 | 14.000 | 16.000 | 18.000 | 19.000 | 20.000 |
|---|---|---|---|---|---|---|---|---|---|---|---|---|
| 17.500 | 0 | | | | | | | | | | | |
| 18.000 | .470 | | | | | | | | | | | |
| 18.500 | .685 | | | | | | | | | | | |
| 19.000 | .825 | | | | | | | | | | | |
| 19.500 | .926 | 0 | | | | | | | | | | |
| 20.000 | 1.010 | .202 | | | | | | | | | | |
| 20.500 | 1.047 | .349 | | | | | | | | | | |
| 21.000 | 1.070 | .459 | | | | | | | | | | |
| 21.500 | 1.089 | .545 | 0 | | | | | | | | | |
| 22.000 | 1.098 | .610 | .122 | | | | | | | | | |
| 23.000 | 1.086 | .691 | .296 | | | | | | | | | |
| 24.000 | 1.050 | .727 | .404 | 24.167=0 | | | | | | | | |
| 25.000 | .996 | .730 | .465 | | | | | | | | | |
| 25.500 | | | | | 0 | | | | | | | |
| 26.000 | .925 | .707 | .490 | .199 | .054 | | | | | | | |
| 27.000 | .858 | .677 | .496 | | .135 | | | | | | | |
| 28.000 | .799 | .647 | .495 | .292 | .190 | | | | | | | |
| 29.000 | .755 | .624 | .492 | | .230 | | | | | | | |
| 29.500 | | | | | | 0 | | | | | | |
| 30.000 | .724 | .608 | .492 | .338 | .261 | .029 | 30.833=0 | | | | | |
| 31.000 | .702 | .598 | .494 | | .286 | .078 | | | | | | |
| 31.500 | | | | | | | | 0 | | | | |
| 32.000 | .685 | .591 | .496 | .370 | .307 | .118 | .055 | .024 | | | | |
| 33.000 | .677 | .590 | .502 | | .328 | .153 | | .066 | | | | |
| 33.500 | | | | | | | | | 0 | | | |
| 34.000 | .670 | .589 | .508 | .399 | .345 | .183 | .129 | .102 | .020 | | | |
| 35.000 | .661 | .585 | .510 | | .359 | .208 | | .132 | .057 | | | |
| 35.500 | | | | | | | | | | 0 | | |
| 36.000 | .640 | .571 | .502 | .409 | .363 | .225 | .179 | .156 | .086 | .017 | | |
| 36.500 | | | | | | | | | | | 0 | |
| 37.000 | .612 | .549 | .486 | | .361 | .235 | | .173 | .110 | .047 | .016 | |
| 37.500 | .594 | .535 | .475 | .396 | .356 | .238 | .198 | .178 | .119 | .059 | .030 | 0 |
| 38.000 | .610 | .547 | .485 | | .360 | .235 | | .172 | .109 | .047 | .016 | |
| 38.500 | | | | | | | | | | | 0 | |
| 39.000 | .631 | .563 | .495 | .404 | .358 | .222 | .176 | .153 | .085 | .017 | | |
| 39.500 | | | | | | | | | | 0 | | |
| 40.000 | .643 | .569 | .496 | | .349 | .202 | | .129 | .055 | | | |
| 41.000 | .649 | .570 | .492 | .386 | .334 | .177 | .124 | .098 | .020 | | | |
| 41.500 | | | | | | | | | 0 | | | |
| 42.000 | .650 | .566 | .482 | | .315 | .147 | | .063 | | | | |
| 43.000 | .649 | .560 | .470 | .351 | .291 | .112 | .052 | .022 | | | | |
| 43.500 | | | | | | | | ) | | | | |
| 44.000 | .655 | .558 | .461 | | .267 | .073 | 44.167=0 | | | | | |
| 45.000 | .667 | .560 | .454 | .311 | .240 | .027 | | | | | | |
| 45.500 | | | | | | 0 | | | | | | |
| 46.000 | .683 | .564 | .445 | | .208 | | | | | | | |
| 47.000 | .710 | .575 | .440 | .259 | .169 | | | | | | | |
| 48.000 | .744 | .587 | .431 | | .117 | | | | | | | |
| 49.000 | .787 | .602 | .417 | .170 | .046 | | | | | | | |
| 49.500 | | | | | 0 | | | | | | | |
| 50.000 | .845 | .620 | .394 | 50.833=0 | | | | | | | | |
| 51.000 | .924 | .640 | .356 | | | | | | | | | |
| 51.500 | .970 | .647 | .323 | | | | | | | | | |
| 52.000 | 1.020 | .649 | .278 | | | | | | | | | |
| 52.500 | 1.048 | .629 | .210 | | | | | | | | | |
| 53.000 | 1.061 | .590 | .118 | | | | | | | | | |
| 53.500 | 1.065 | .533 | 0 | | | | | | | | | |
| 54.000 | 1.060 | .454 | | | | | | | | | | |
| 54.500 | 1.045 | .348 | | | | | | | | | | |
| 55.000 | 1.011 | .202 | | | | | | | | | | |
| 55.500 | .942 | 0 | | | | | | | | | | |
| 56.000 | .842 | | | | | | | | | | | |
| 56.500 | .712 | | | | | | | | | | | |
| 57.000 | .500 | | | | | | | | | | | |
| 57.500 | 0 | | | | | | | | | | | |

23



$A = 2$
$b/2 = 20$
$l = 60$
$C_R = 40$
$S_W = 800$ sq in.
$\bar{c} = 26.67$

dimensions in inches

45°

45°

Sta. 57.50

Sta. 55.64

Sta. 19.36

Moment center

Sta. 34.50

17.50

Sta. 0

(a) Complete model.

Figure 1.- Sketch of the model.
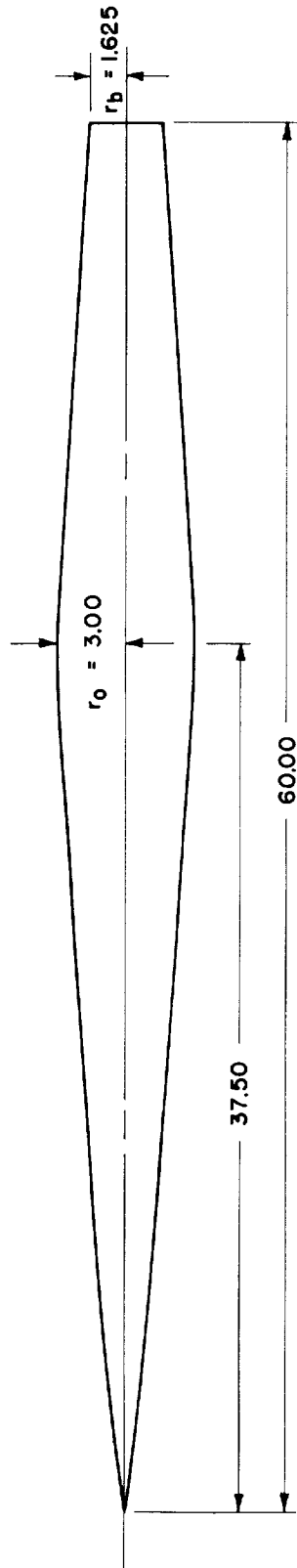
(b) Equivalent body.

Figure 1.- Concluded.
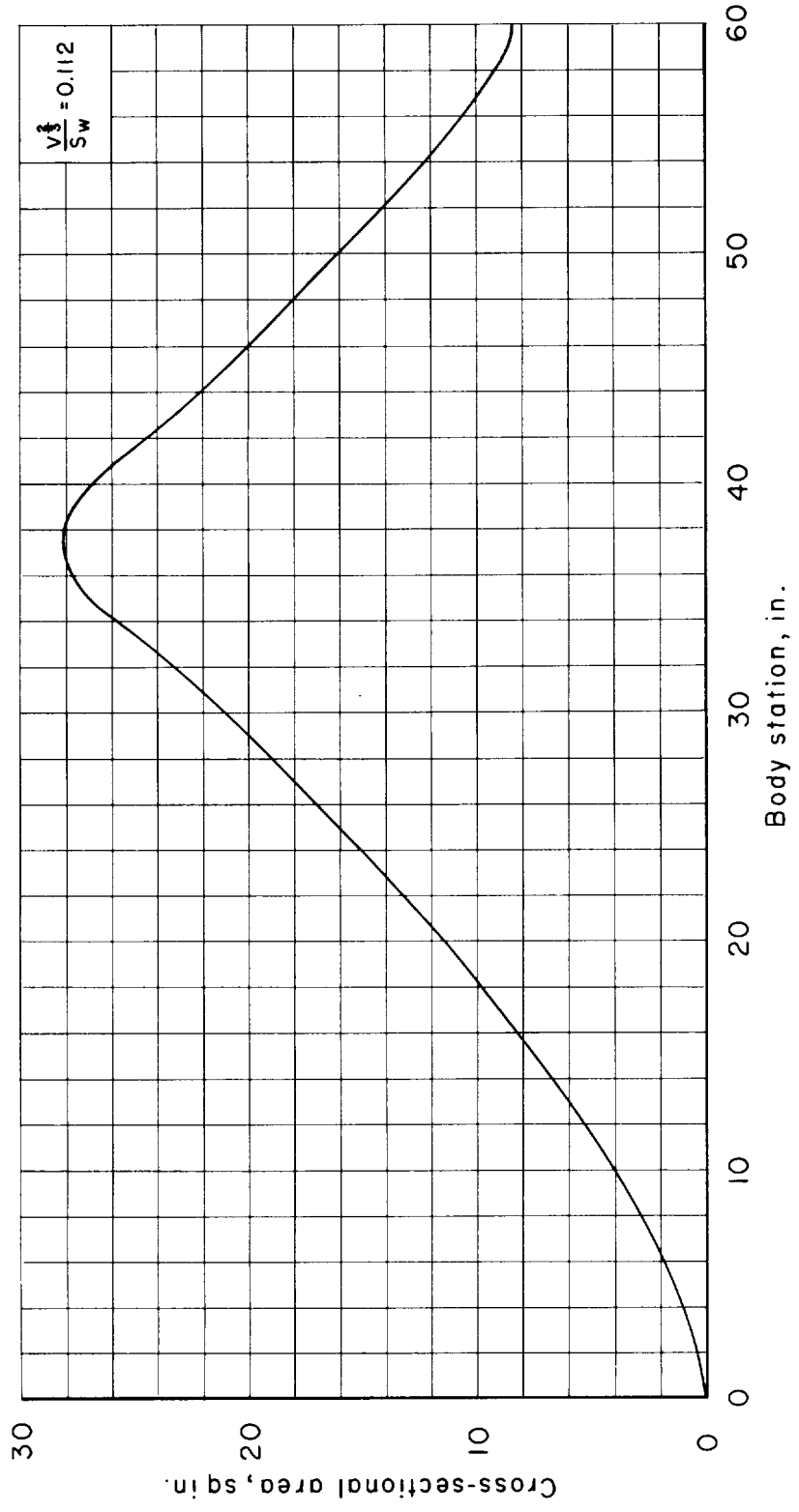
Figure 2.- Design area distribution, $KA_{25}$.
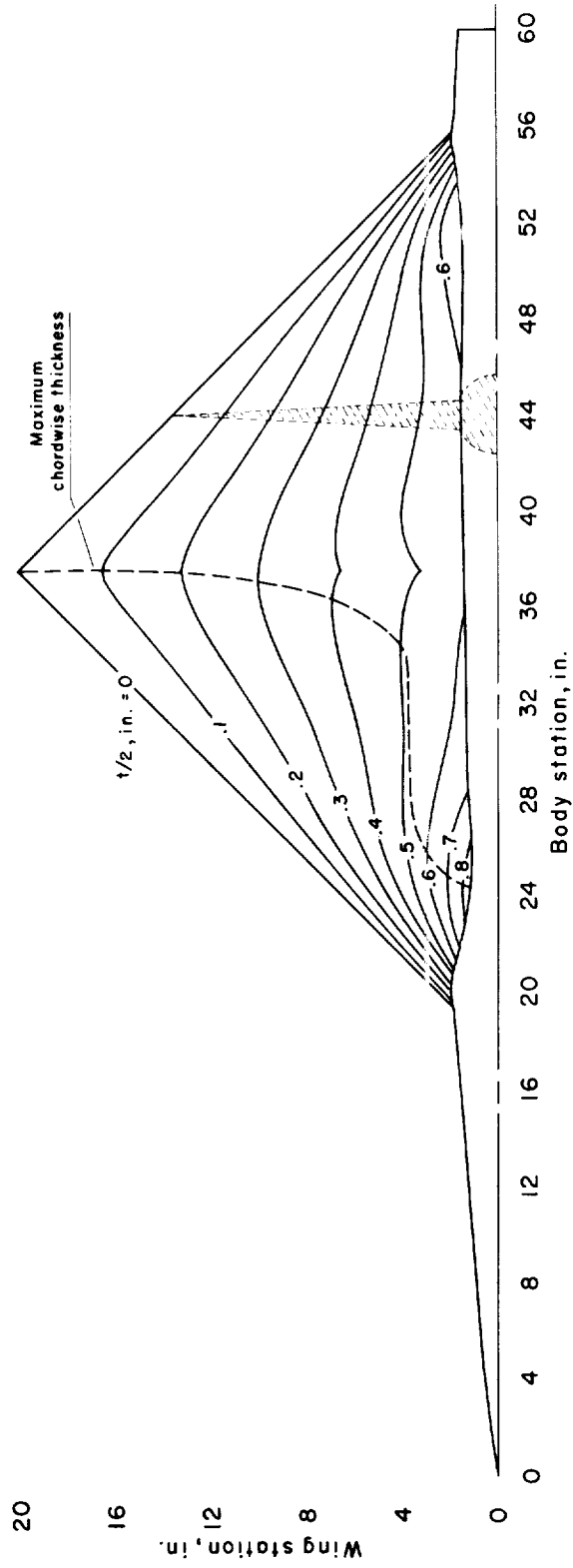
Figure 3.- Semi-plan view of the diamond model with wing thickness contours.

A-23674

Figure 4.- Diamond model in the 8- by 7-foot supersonic test section of the Ames Unitary Plan wind tunnel.
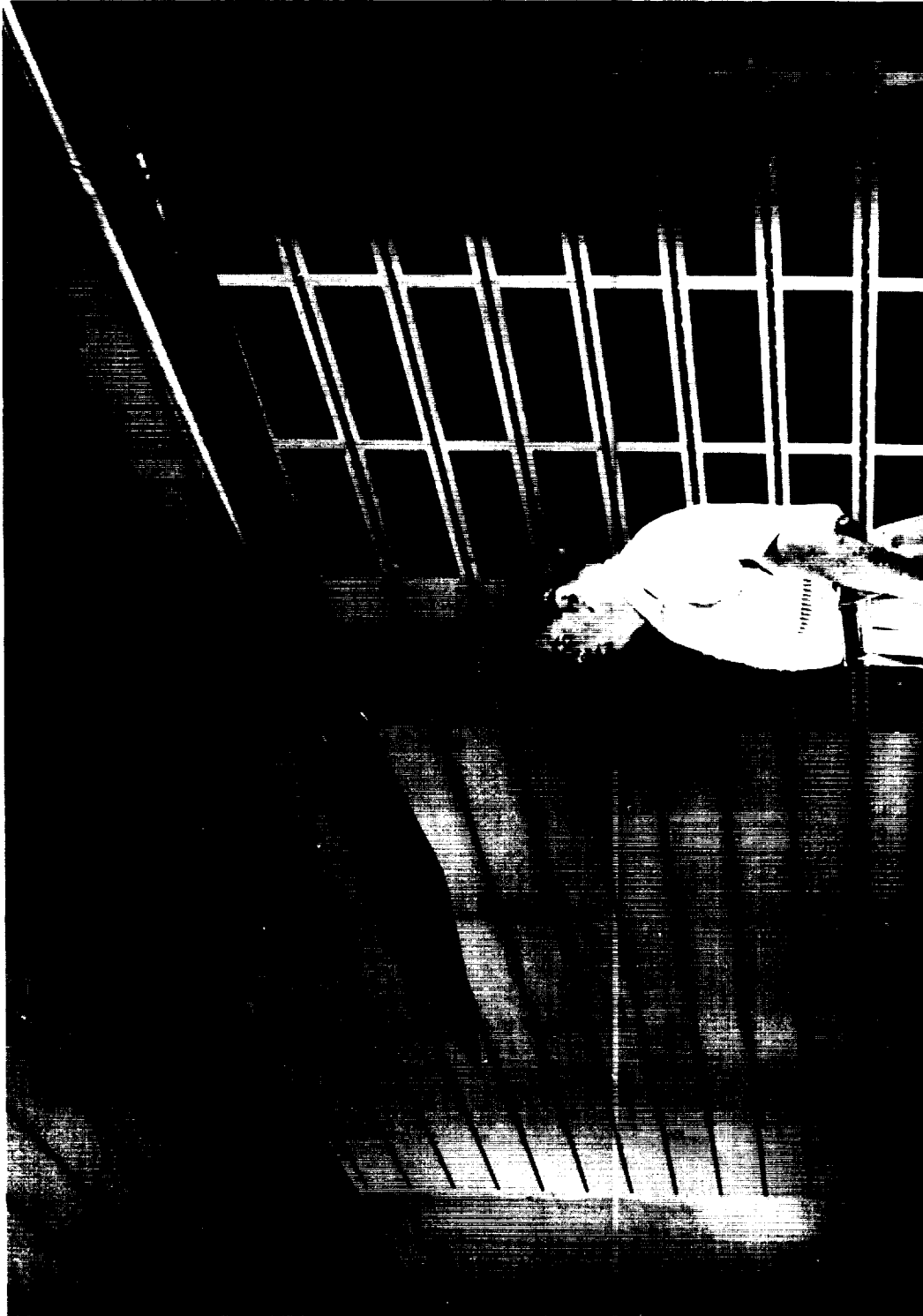
Figure 5.- Equivalent body ($KA_{25}$ area distribution) in the test section of the Ames 14-foot transonic wind tunnel.

A-23952
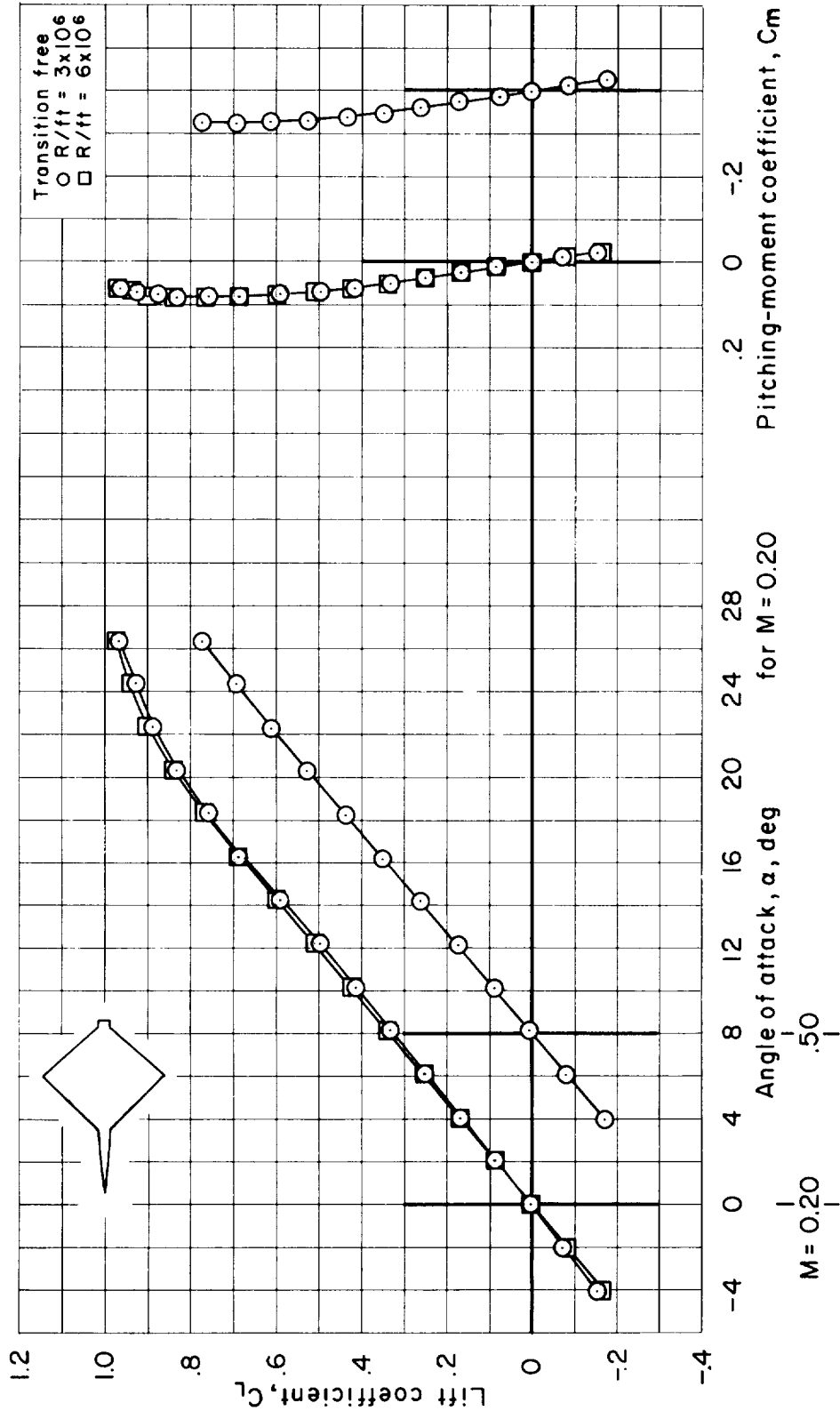
(a) $C_L$ vs. $\alpha$ and $C_m$

Figure 6.- Subsonic aerodynamic characteristics of the diamond model with transition free as determined from tests in the Ames 12-foot pressure wind tunnel.

30
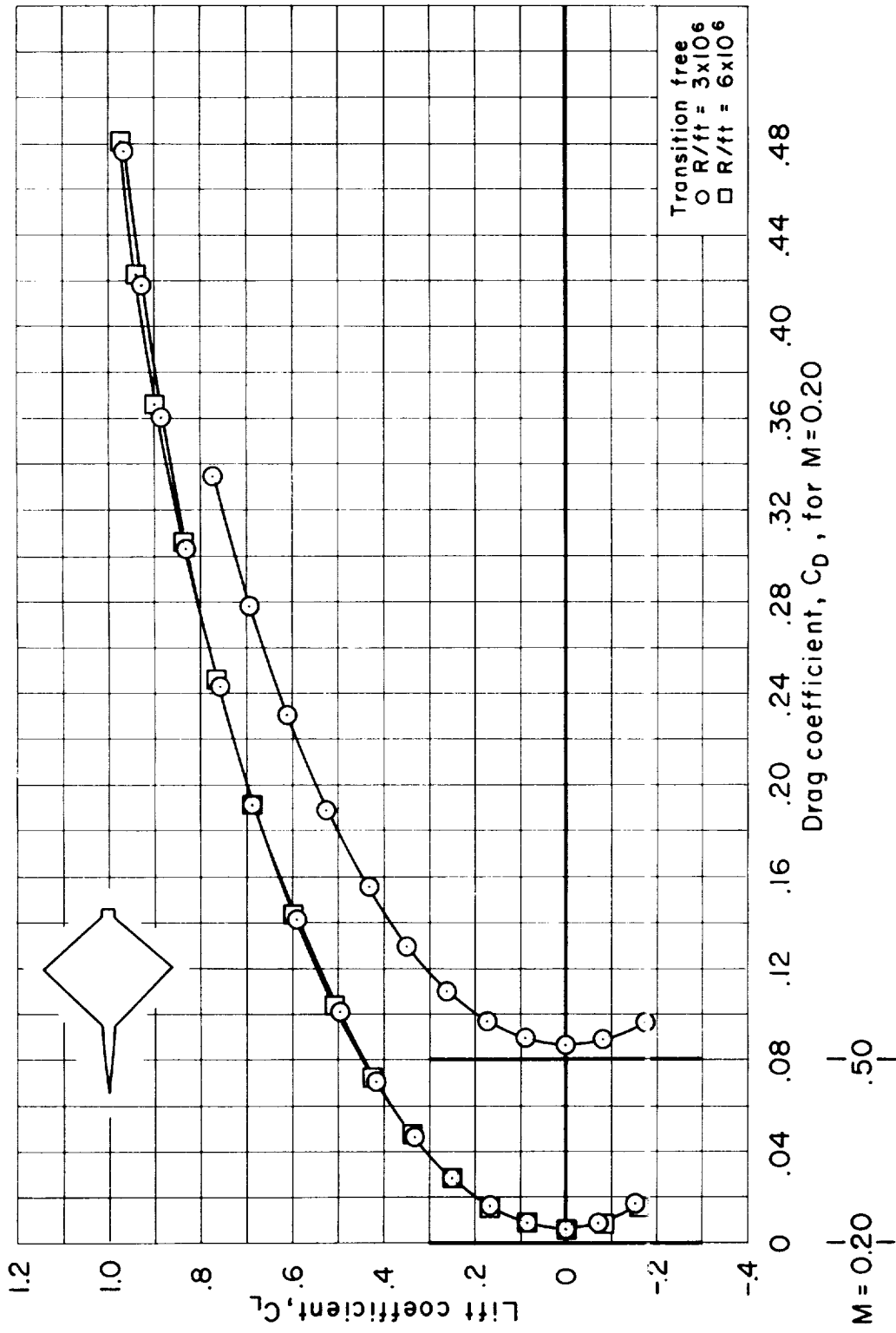


(b) $C_L$ vs. $C_D$

Figure 6.— Concluded.
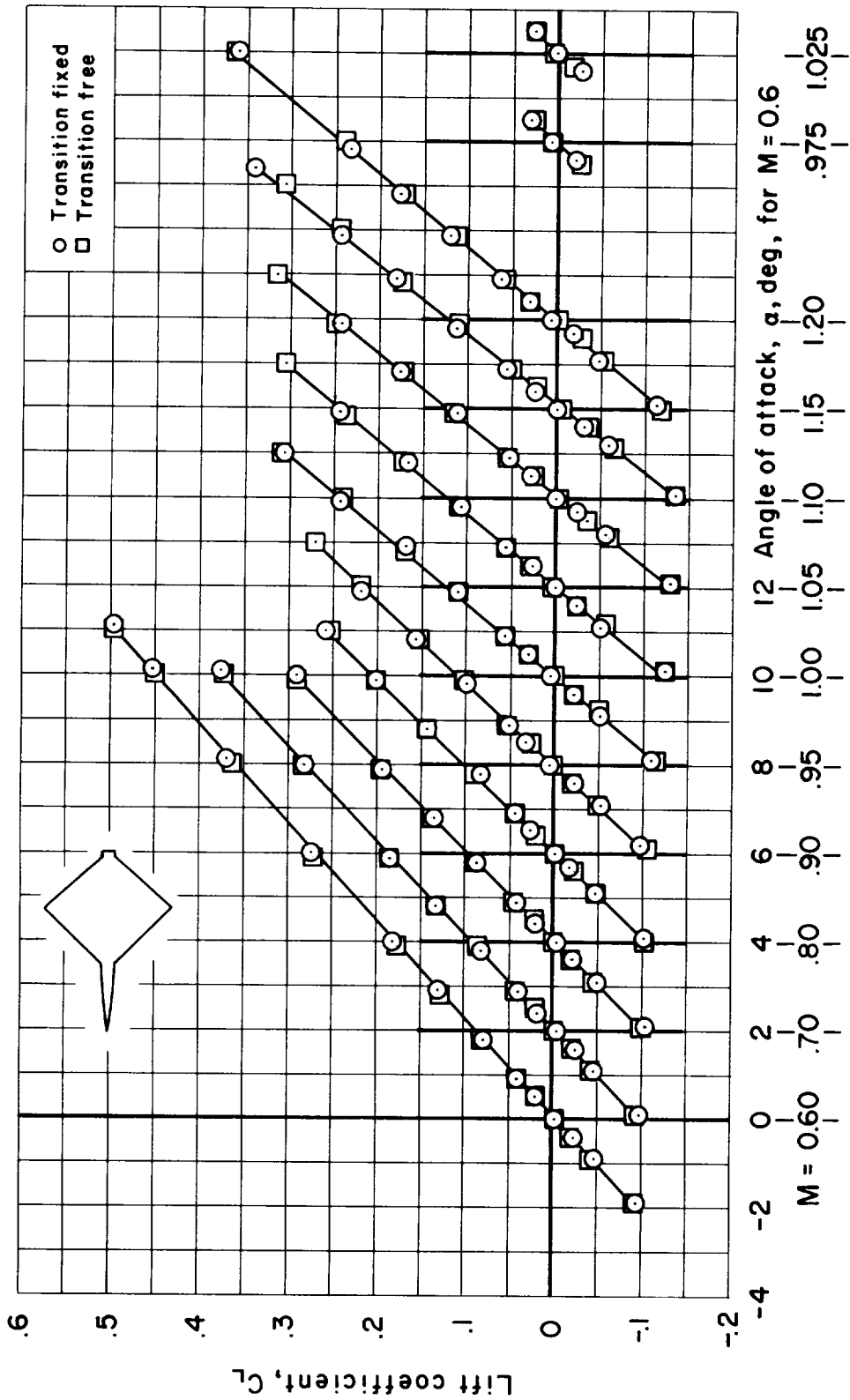
(a) $C_L$ vs. $\alpha$

Figure 7.— Transonic aerodynamic characteristics of the diamond model with transition fixed and free as determined from tests in the Ames 14-foot transonic wind tunnel.
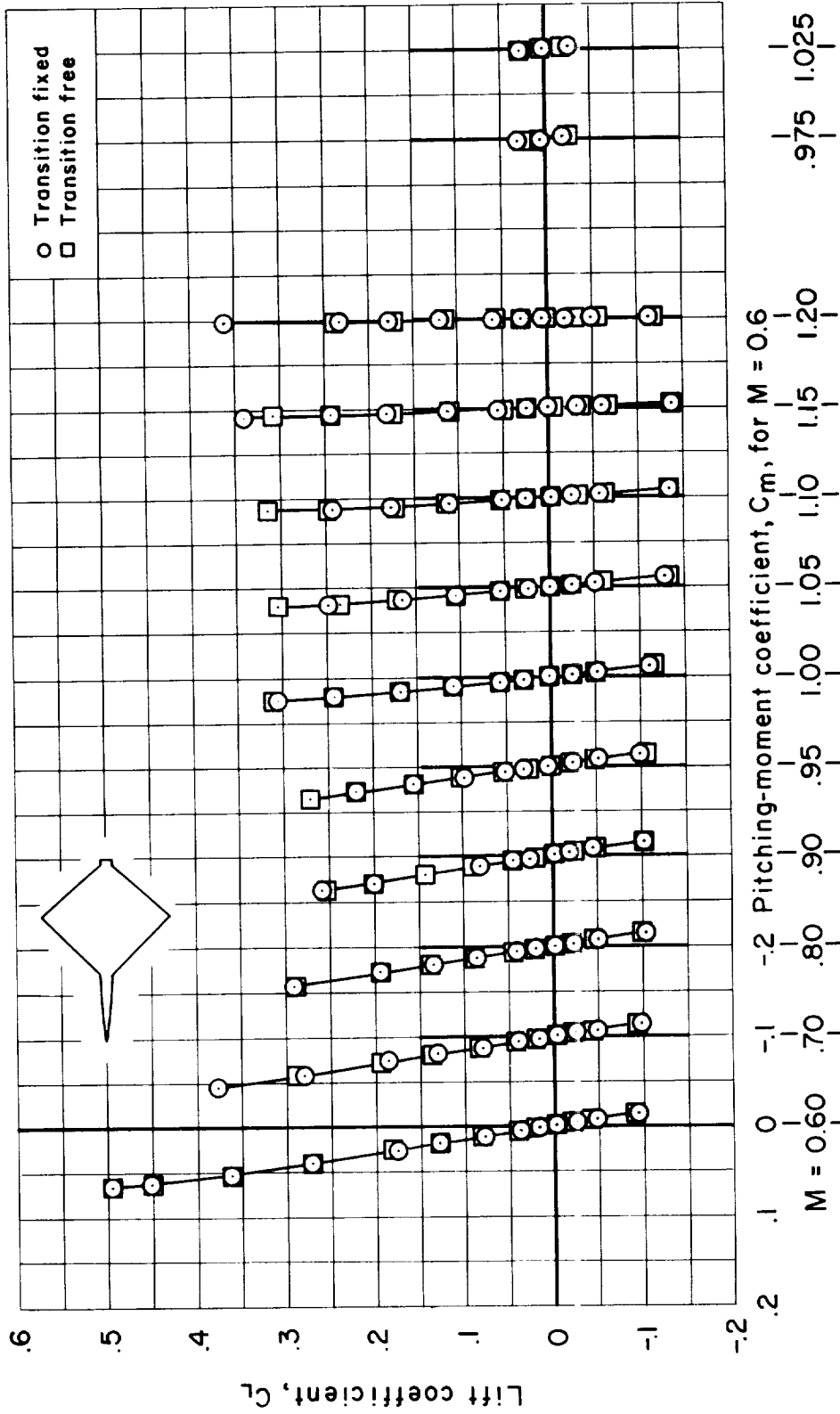
(b) $C_L$ vs. $C_m$

Figure 7.- Continued.

A-201
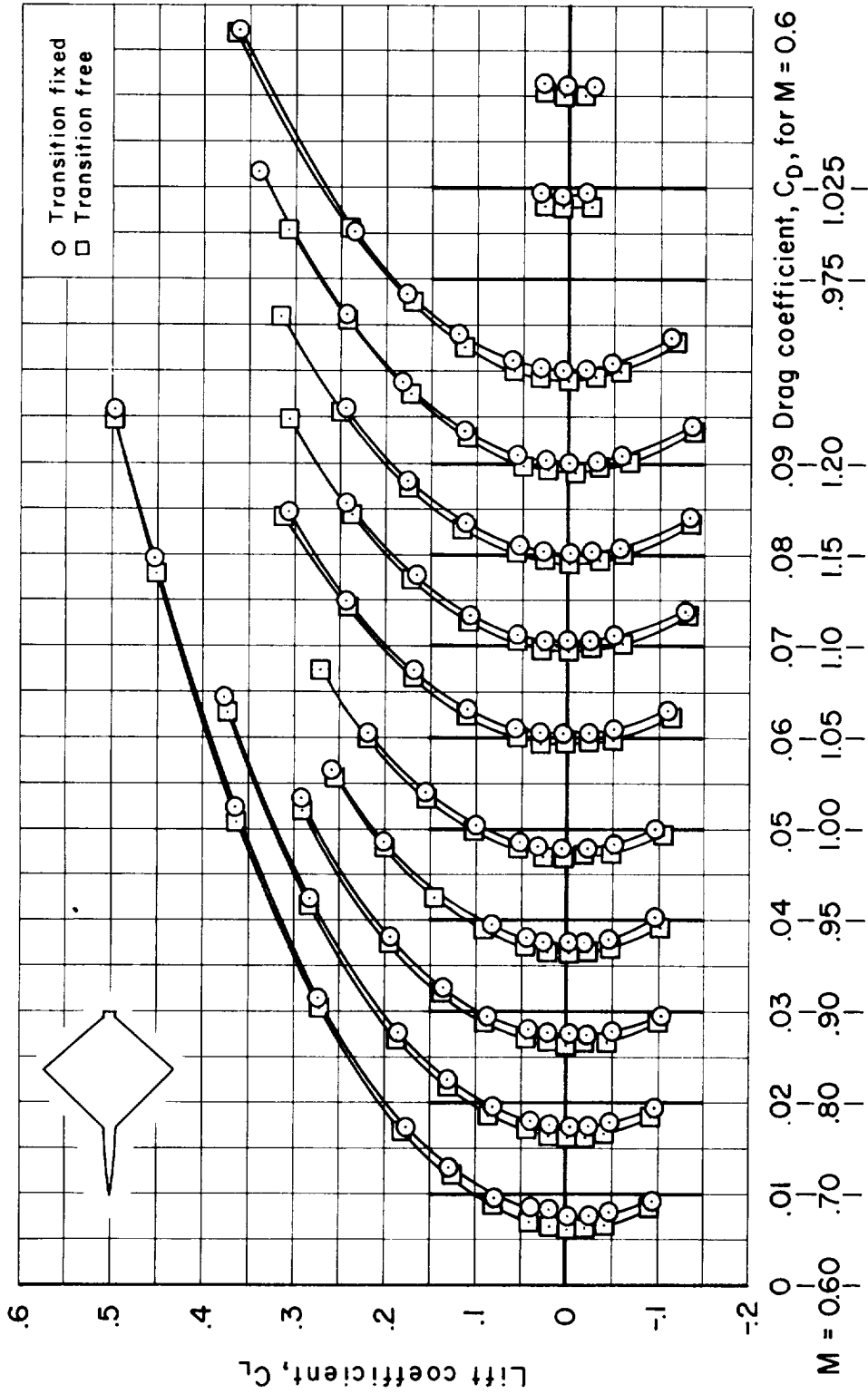


(c) $C_L$ vs. $C_D$

Figure 7.- Concluded.
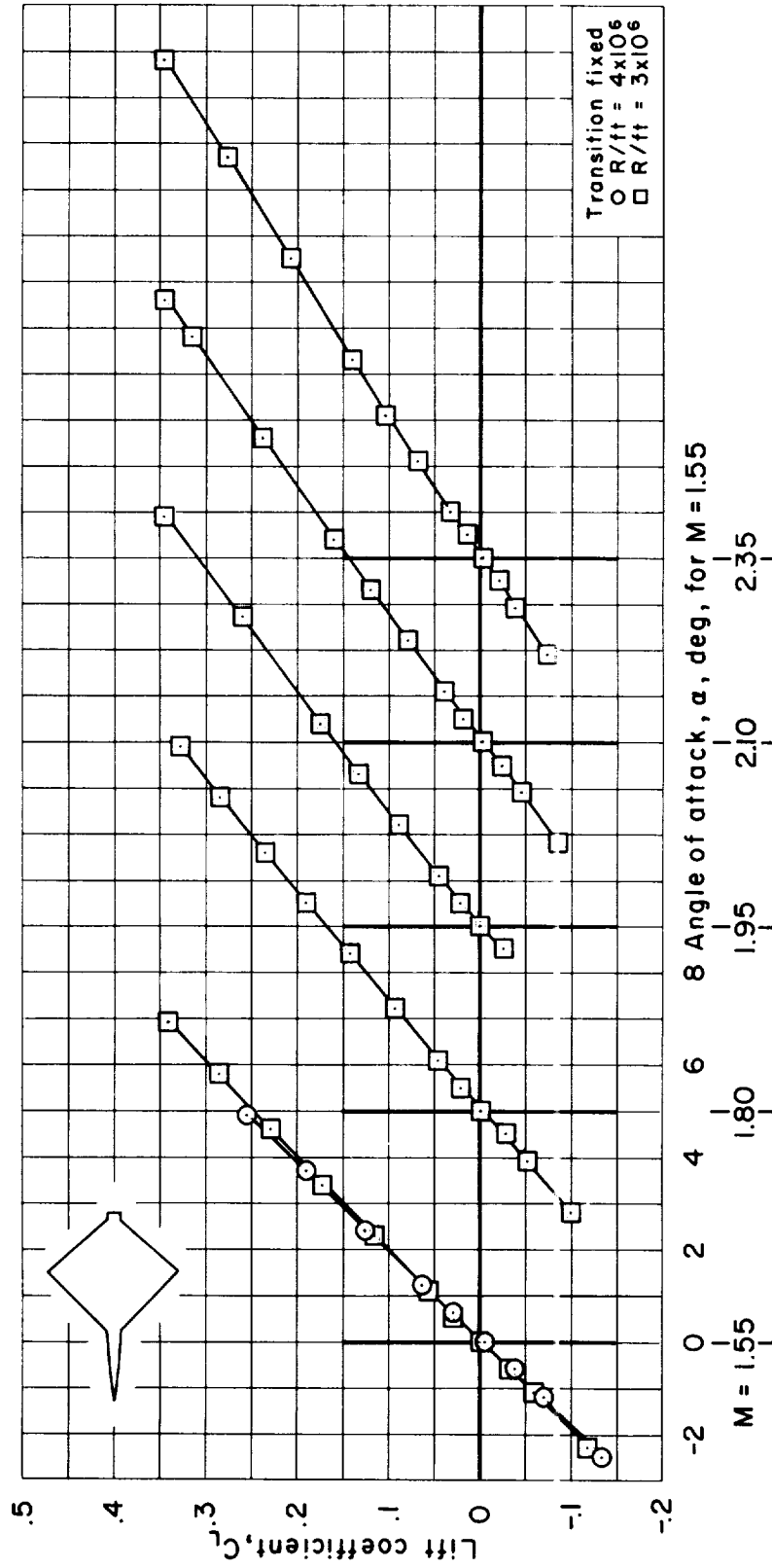
(a) $C_L$ vs. $\alpha$

Figure 8.- Supersonic aerodynamic characteristics of the diamond model with transition fixed as determined from tests in the 9- by 7-foot supersonic test section of the Ames Unitary Plan wind tunnel.
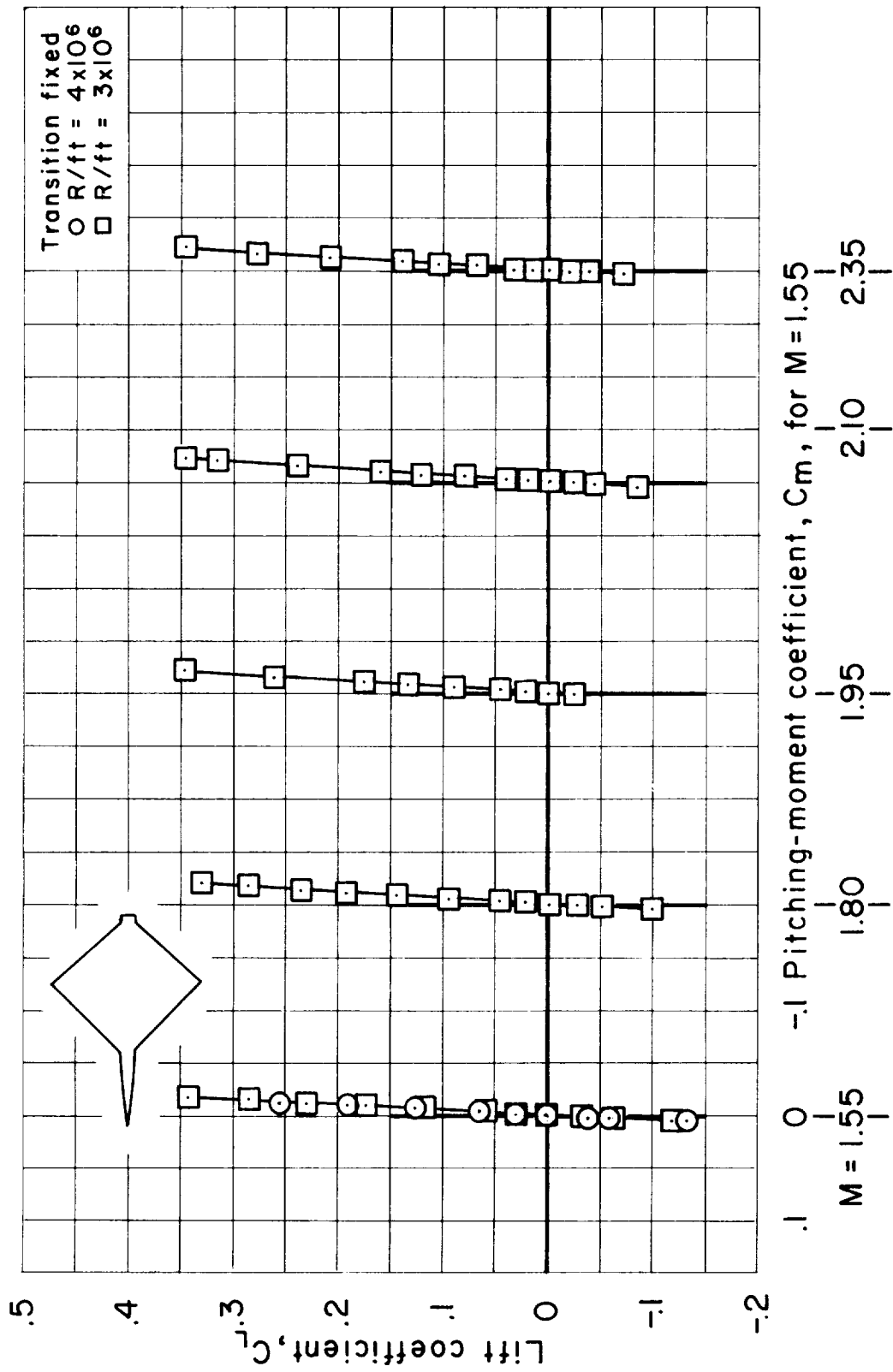
(b) $C_L$ vs. $C_m$

Figure 8.- Continued.

36
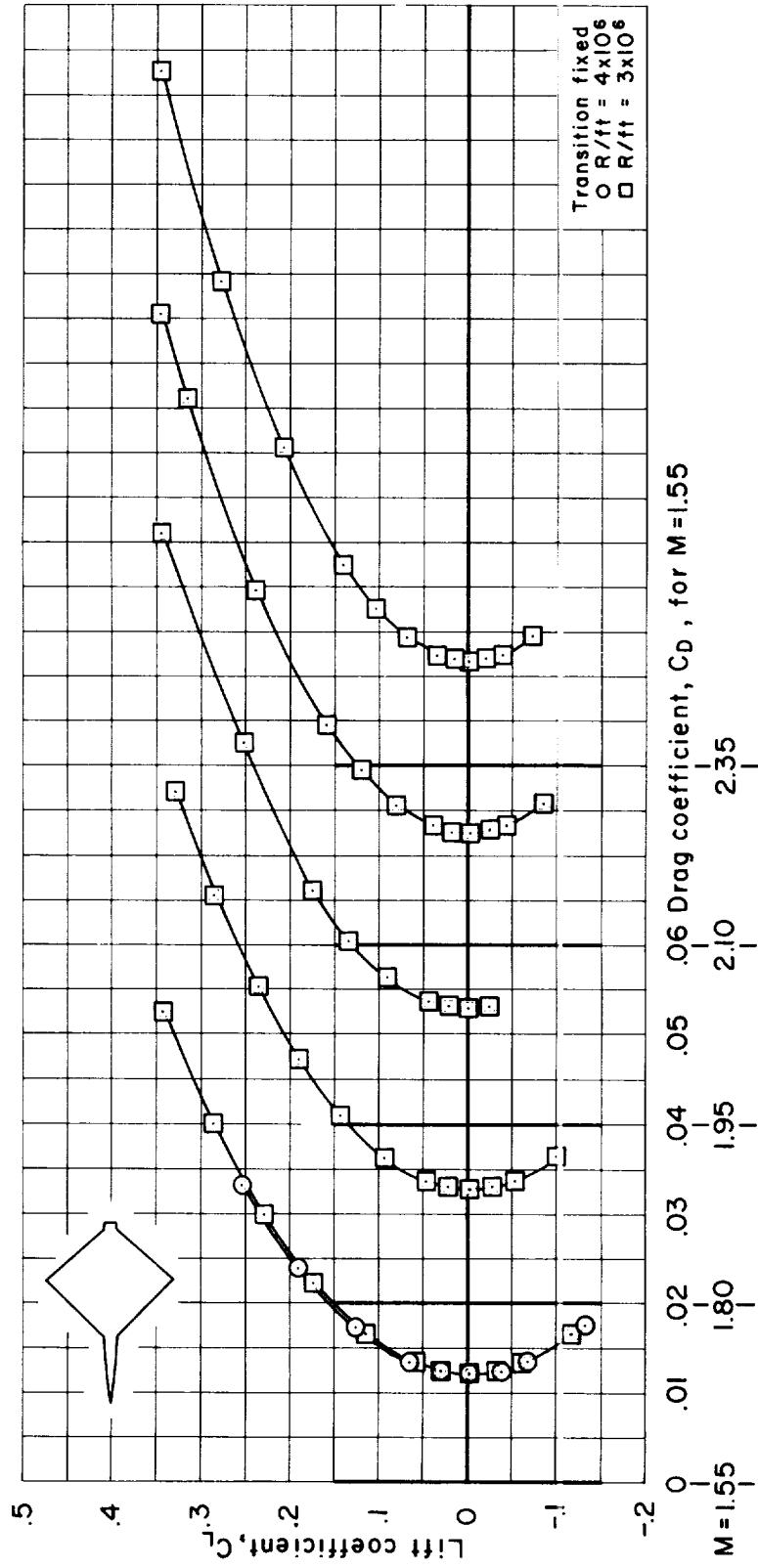


(c) $C_L$ vs. $C_D$

Figure 8.- Concluded.
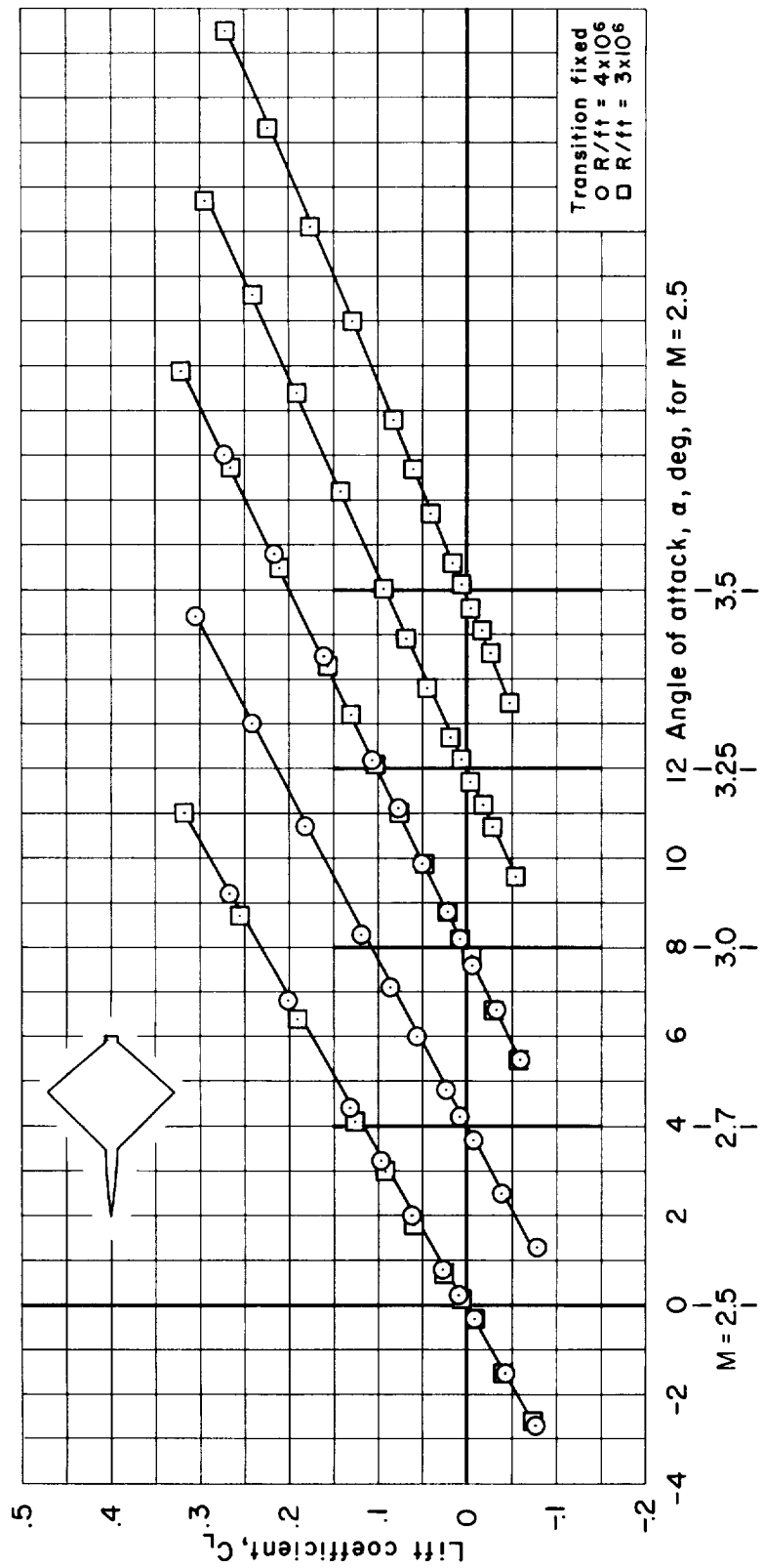
(a) $C_L$ vs. $\alpha$, transition fixed

Figure 9.- Supersonic aerodynamic characteristics of the diamond model with transition fixed and free as determined from tests in the 8- by 7-foot supersonic test section of the Ames Unitary Plan wind tunnel.
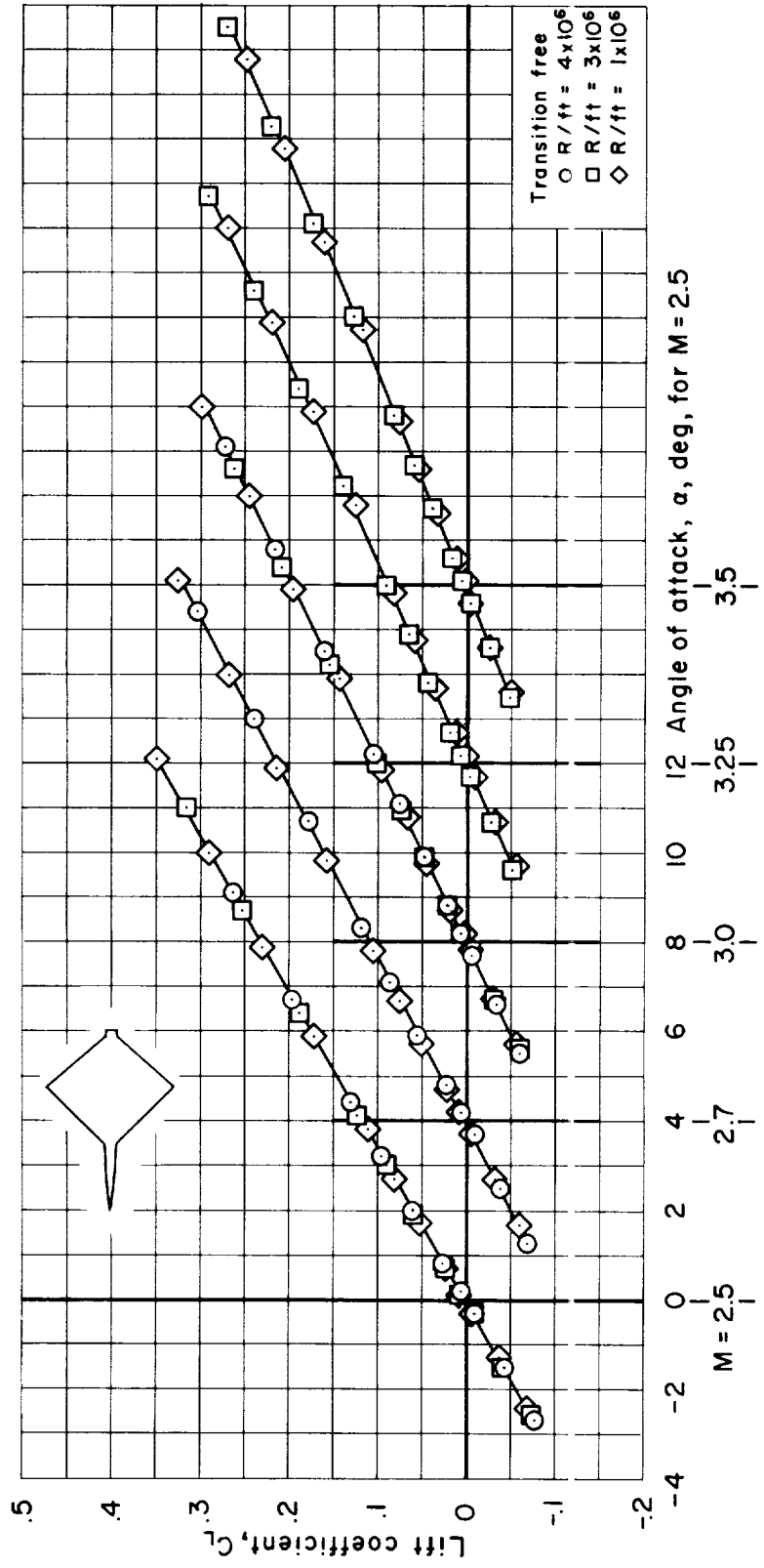
(b) $C_L$ vs. $\alpha$, transition free

Figure 9.- Continued.
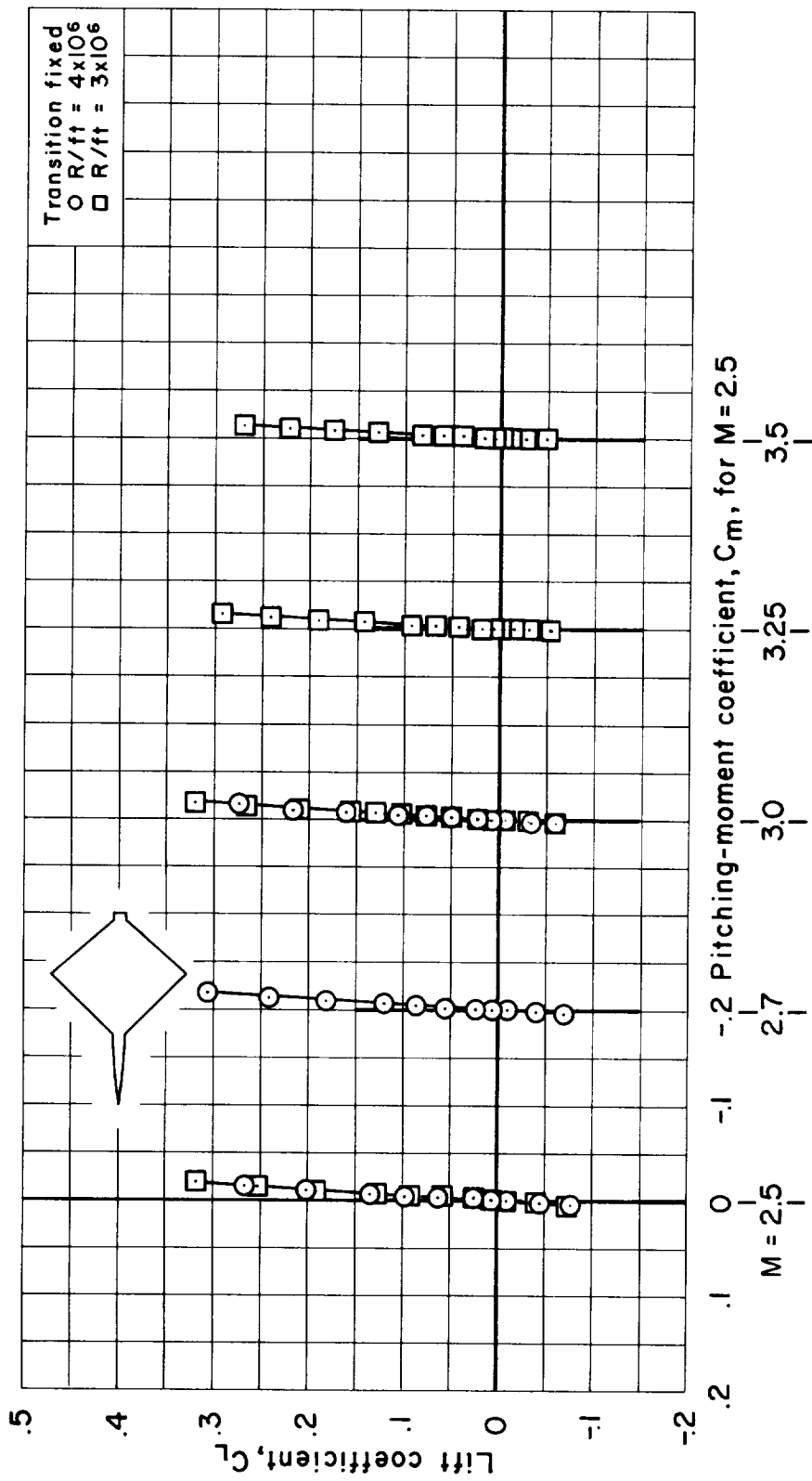
(c) $C_L$ vs. $C_m$, transition fixed

Figure 9.- Continued.

40
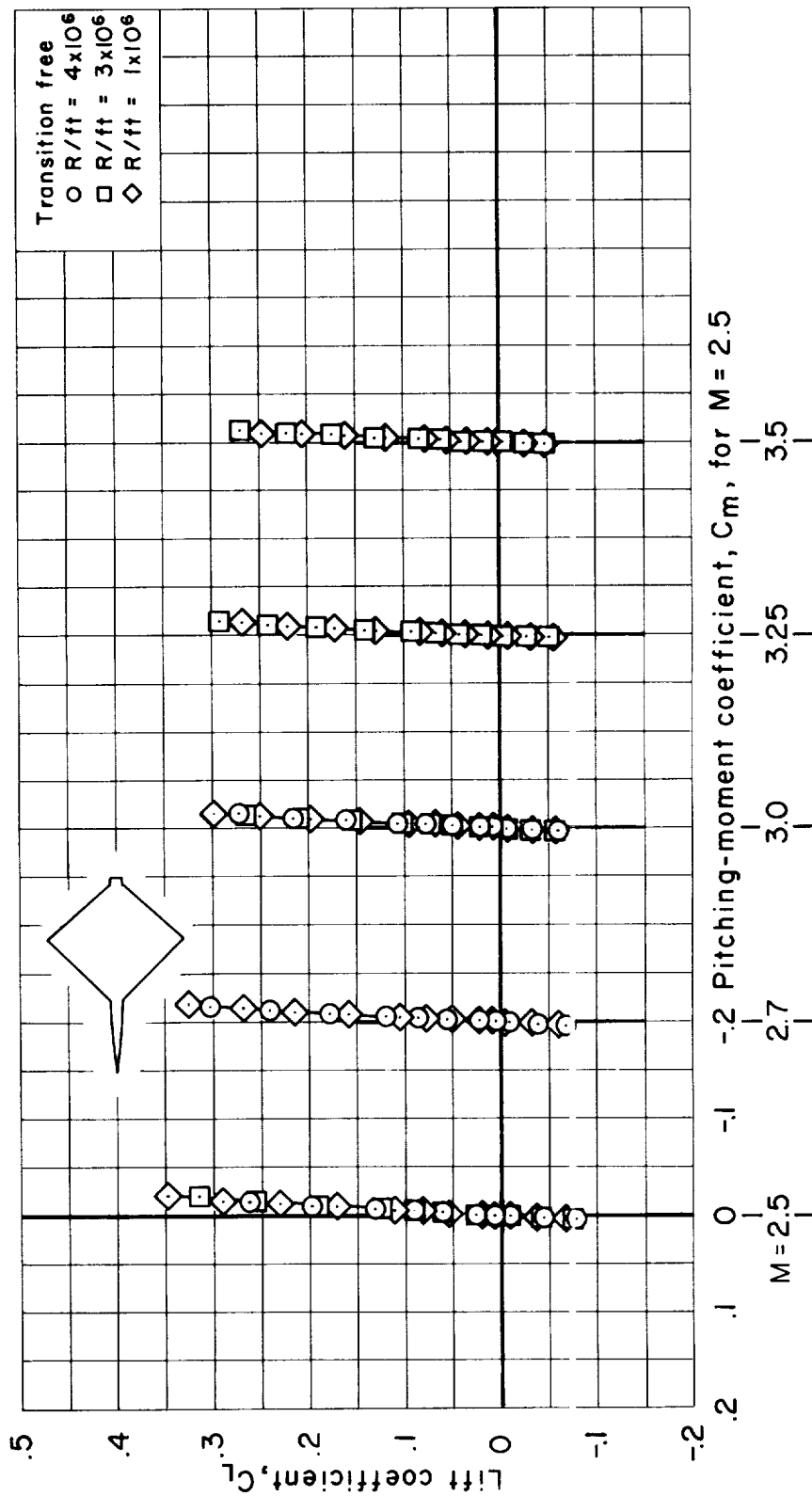


(d) $C_L$ vs. $C_m$, transition free

Figure 9.- Continued.
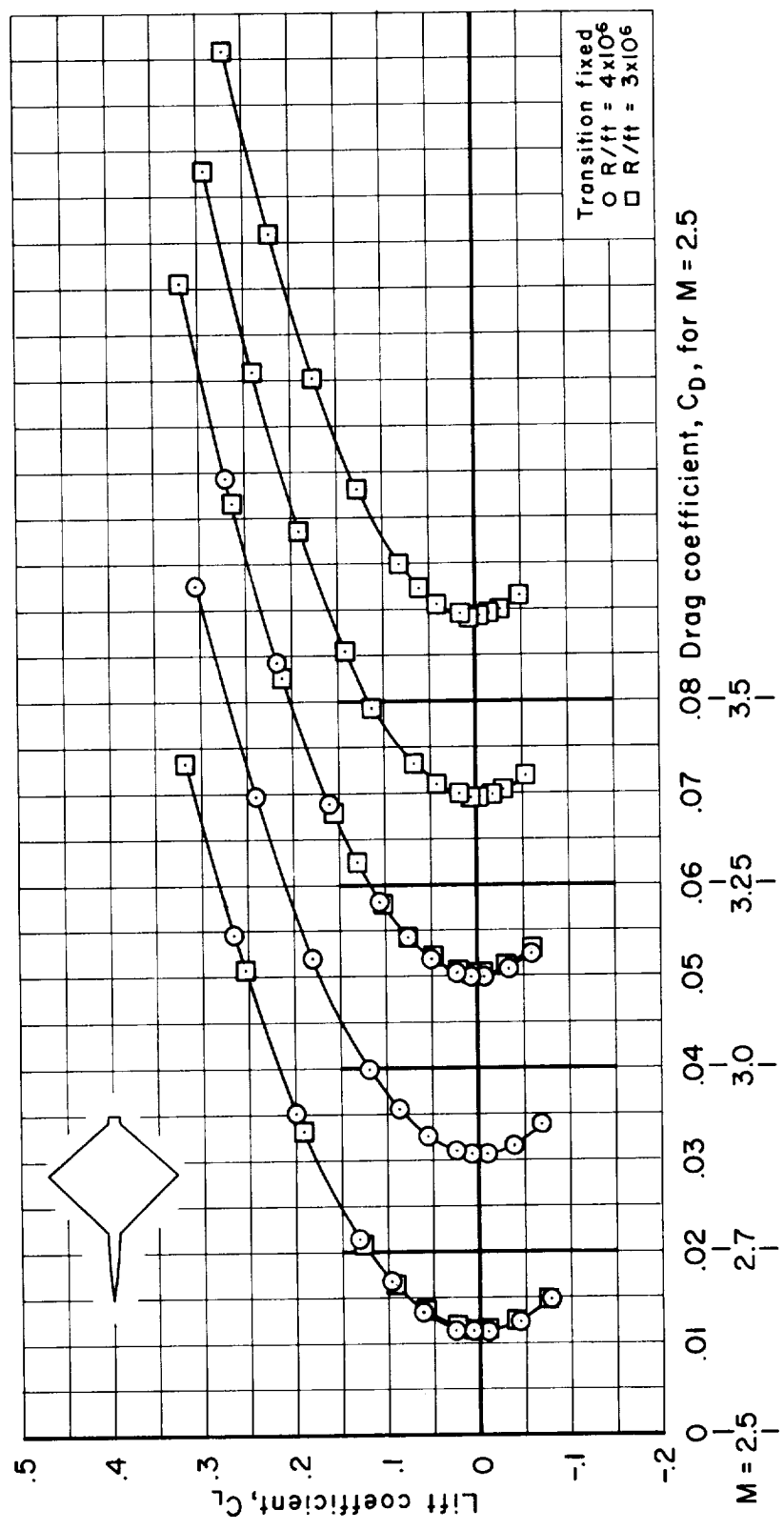
(e) $C_L$ vs. $C_D$, transition fixed

Figure 9.- Continued.
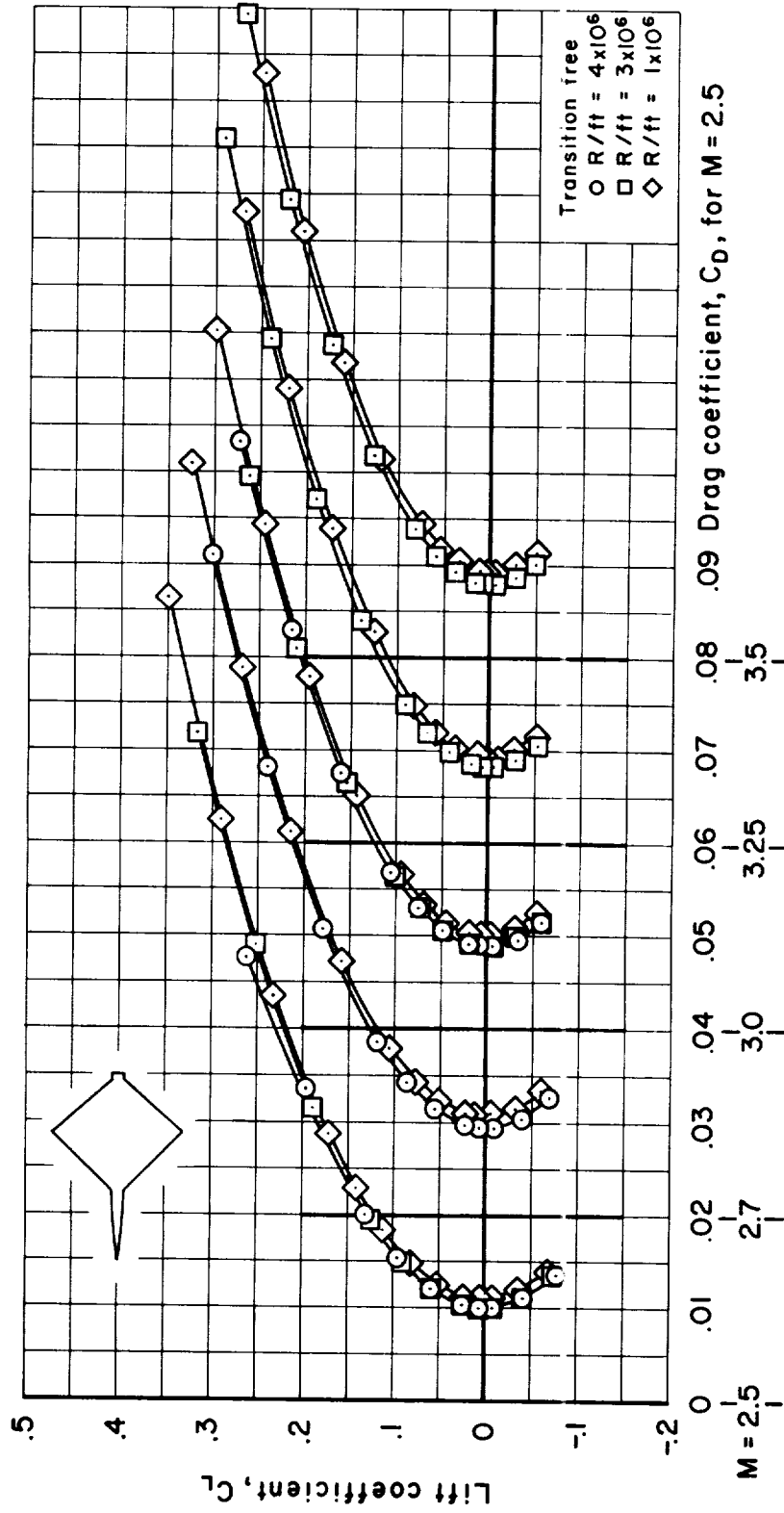
(f) $C_L$ vs. $C_D$, transition free

Figure 9.- Concluded.
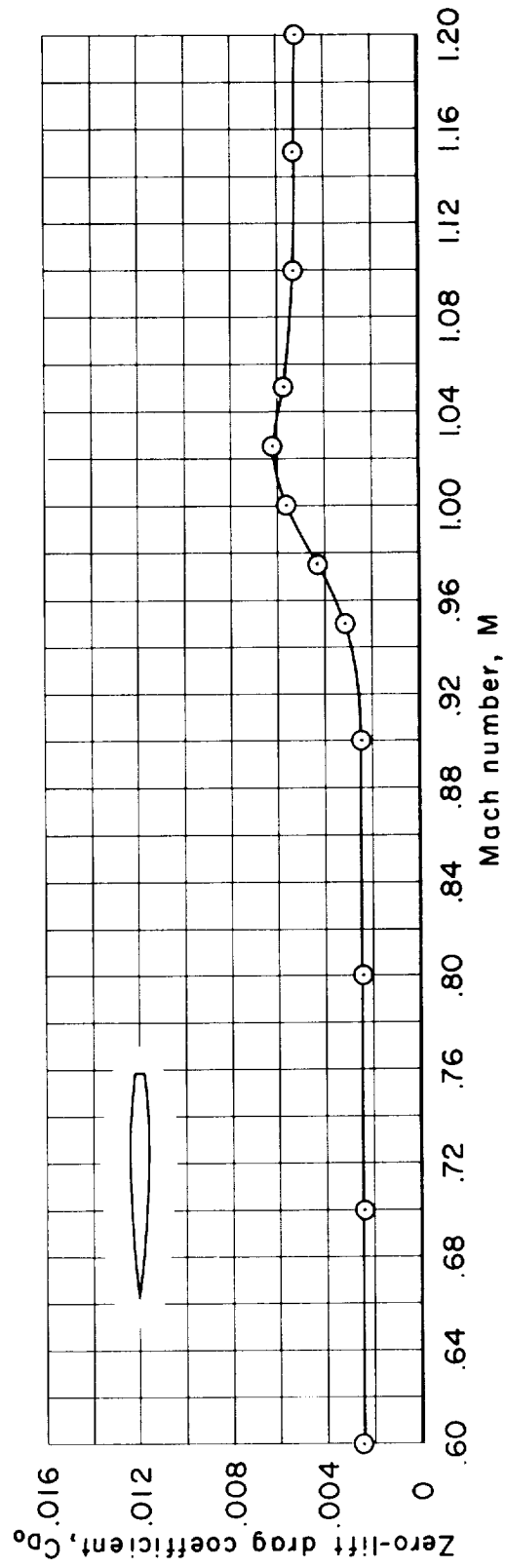
Figure 10.- Zero-lift drag coefficients for the $M = 1.00$ equivalent body ($KA_{25}$ area distribution) as determined from tests in the Ames 14-foot transonic wind tunnel.

44
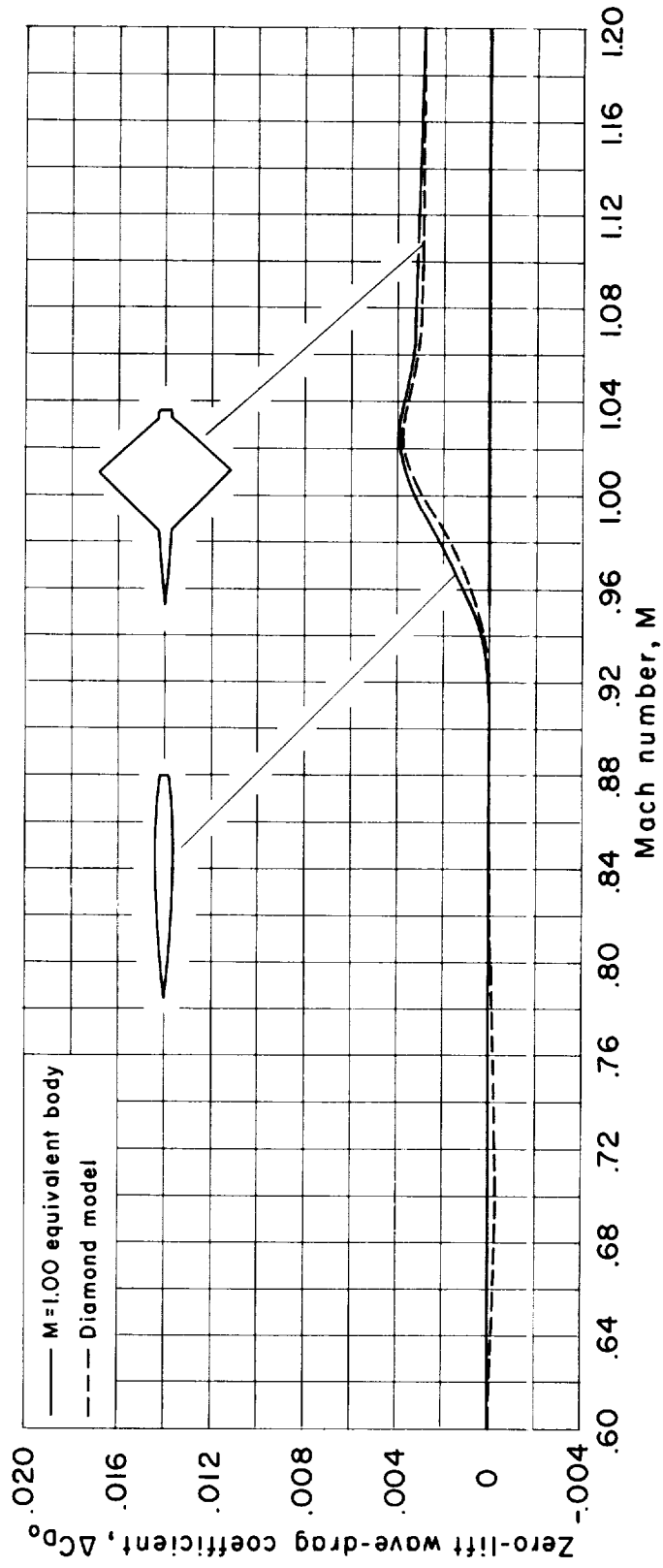


Figure 11.- Zero-lift wave-drag coefficients for the diamond model and its M = 1.00 equivalent body.
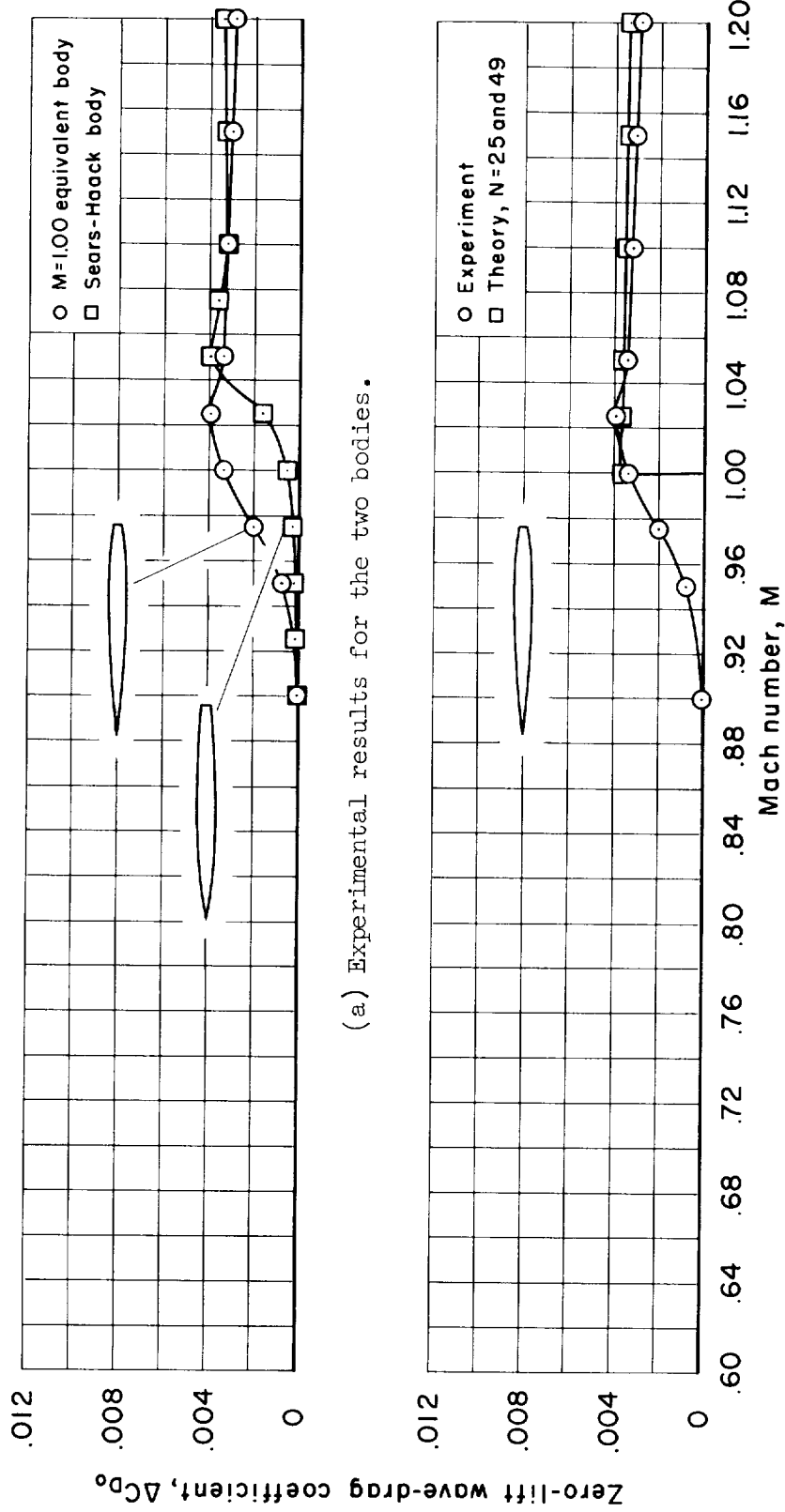
(a) Experimental results for the two bodies.

(b) Experiment and theory, M = 1.00 equivalent body.

Figure 12.— Zero-lift wave-drag coefficients for the M = 1.00 equivalent body $(KA_{25})$ and a minimum-wave-drag body for prescribed volume and length (Sears-Haack).
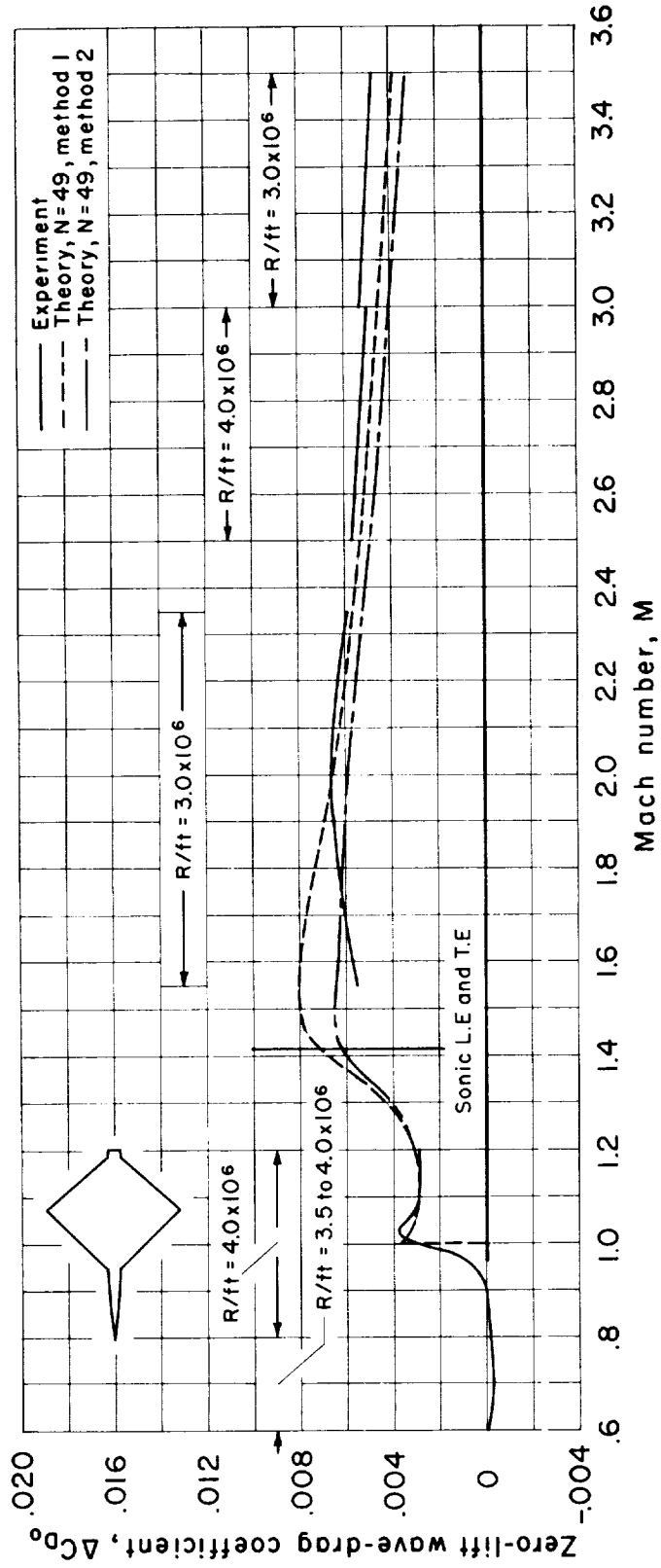
Figure 13.- Zero-lift wave-drag coefficients of the diamond model as determined by experiment and theory.
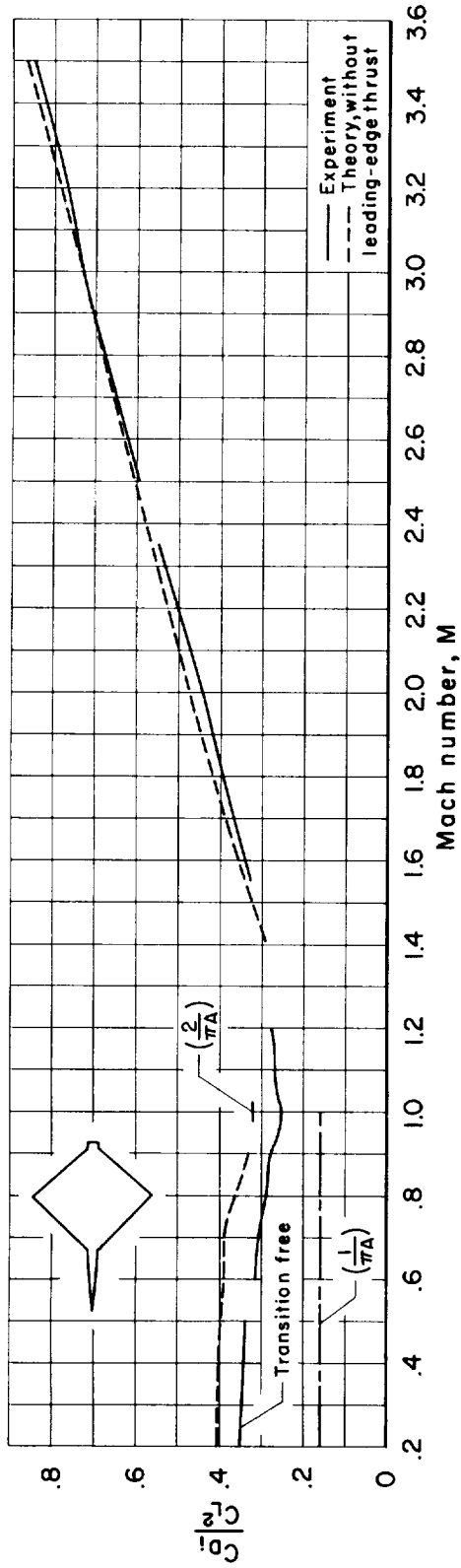
(a) Drag due to lift parameter.
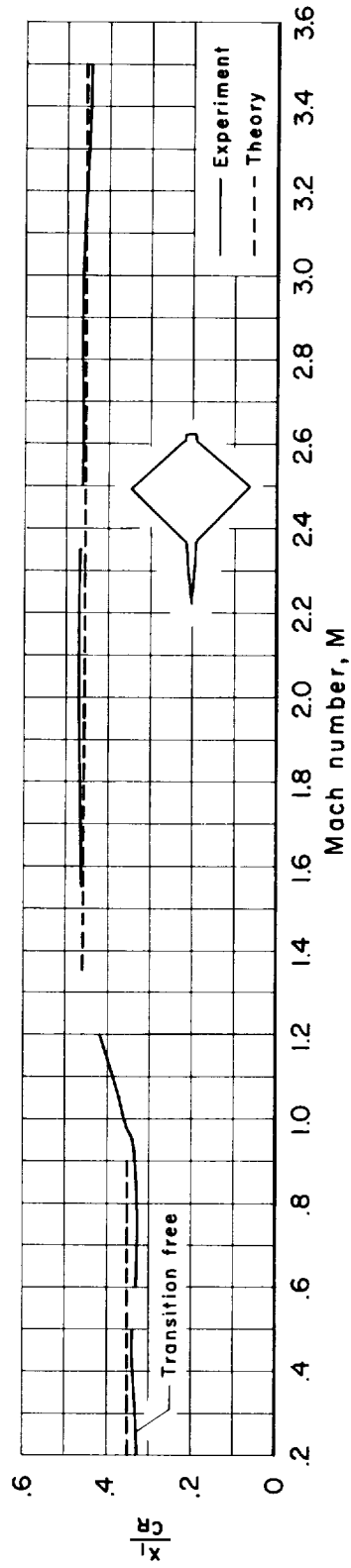
(b) Aerodynamic center location.

Figure 14.- Aerodynamic trends with Mach number for the diamond model as indicated by experiment and theory (transition fixed except as noted).

47
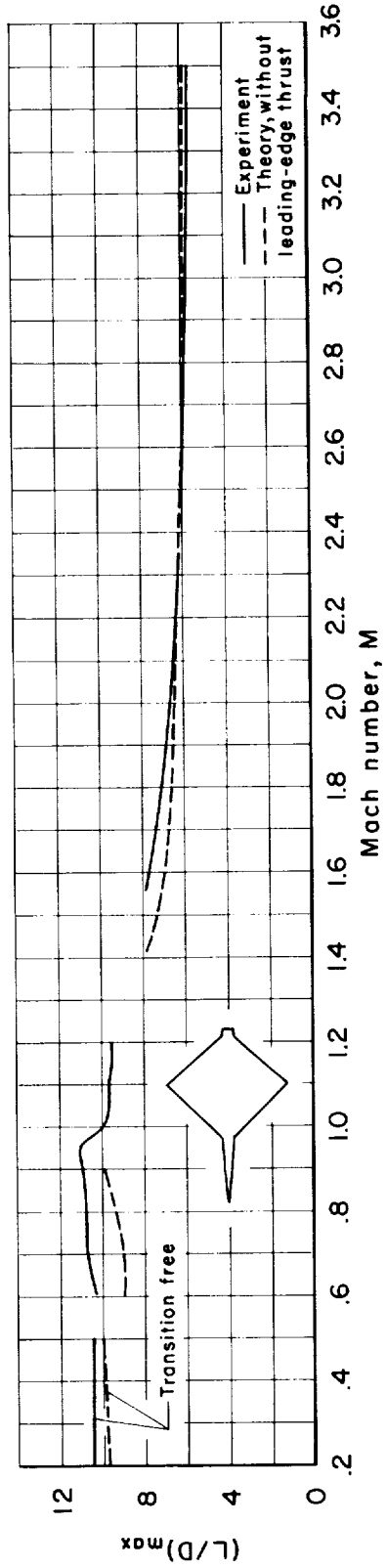
(c) Maximum lift-drag ratio.
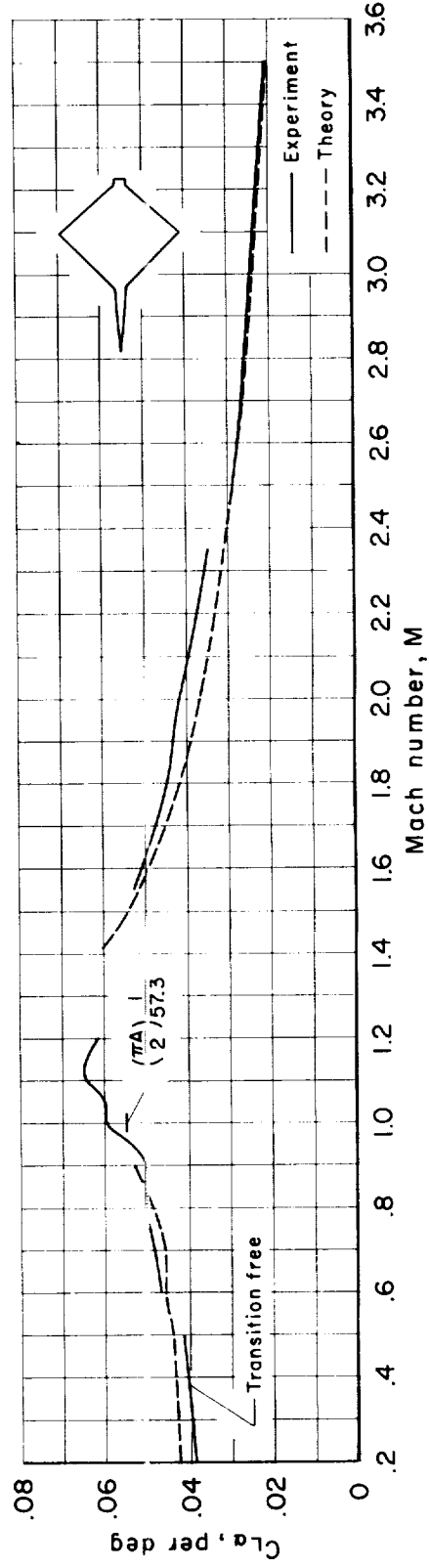
(d) Lift-curve slope, per deg.

Figure 14.- Concluded.

$$S = \frac{l}{4}\sum_{2}^{N} A_n \left[\frac{\sin(n-1)\phi}{n-1} - \frac{\sin(n+1)\phi}{n+1}\right] \; ; \; \cos\phi = \left(\frac{2x}{l}-1\right)$$

$V/V_{A_2} = 0.68$

$A_N$

$\Delta C_{D_0} = 0.0034$

$V/V_{A_2} = 0.83$

$A_2 = 1.405$
$A_4 = -0.727$
$\Delta C_{D_0} = 0.0026$

$V/V_{A_2} = 0.91$

$A_2 = 1.551$
$A_4 = -0.360$
$\Delta C_{D_0} = 0.0023$

$V/V_{A_2} = 1.00$

$A_2 = 1.696$
$\Delta C_{D_0} = 0.0025$

$V/V_{A_2} = 0.91$

$A_2 = 1.551$
$A_3 = 0.836$
$\Delta C_{D_0} = 0.0030$

$V/V_{A_2} = 0.91$

$A_2 = 1.551$
$A_3 = -0.836$
$\Delta C_{D_0} = 0.0030$

Cross-sectional area, S, sq in.
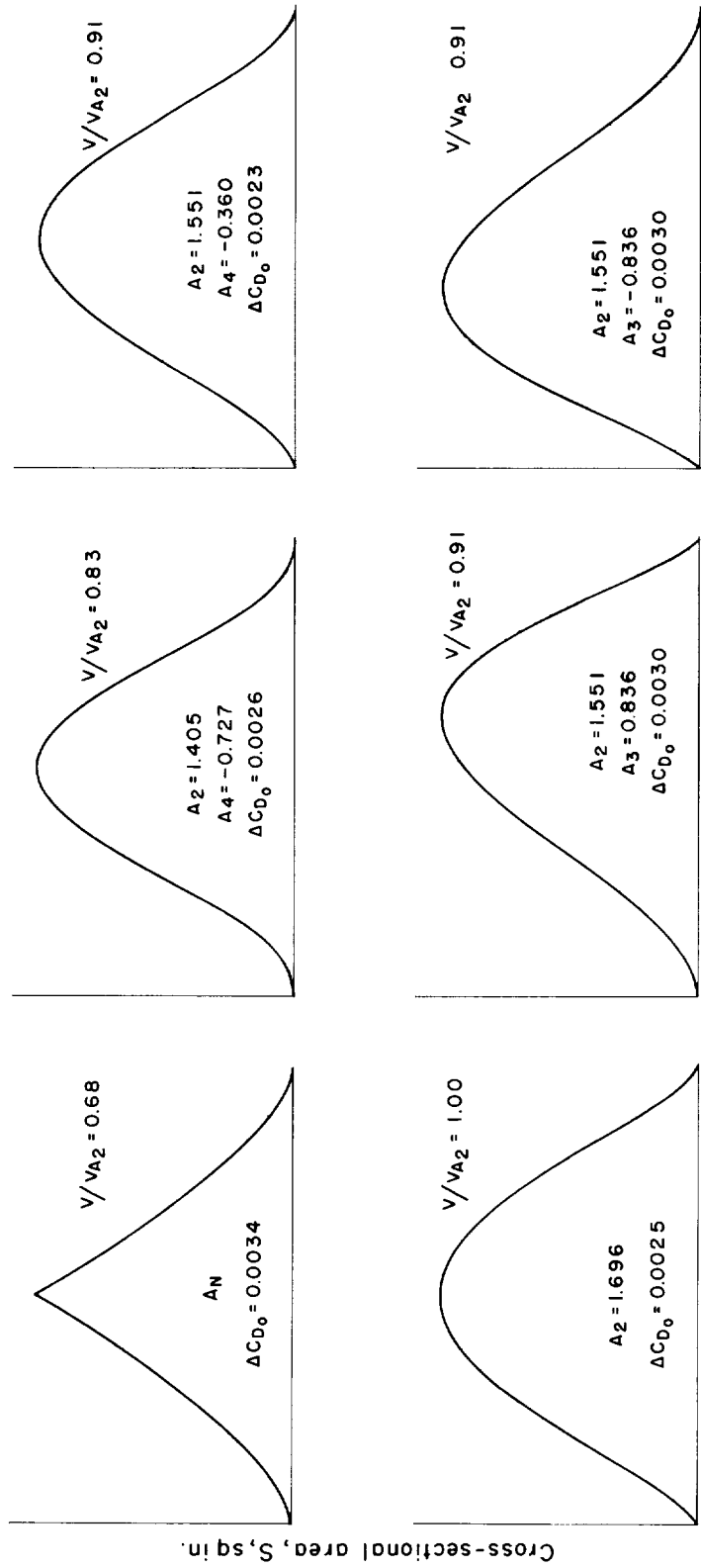
Body station, x, in.

Figure 15.- Area curves considered in the selection of the design area distribution; the corresponding theoretical (N = 25) zero-lift wave-drag coefficients are for M = 1.00.
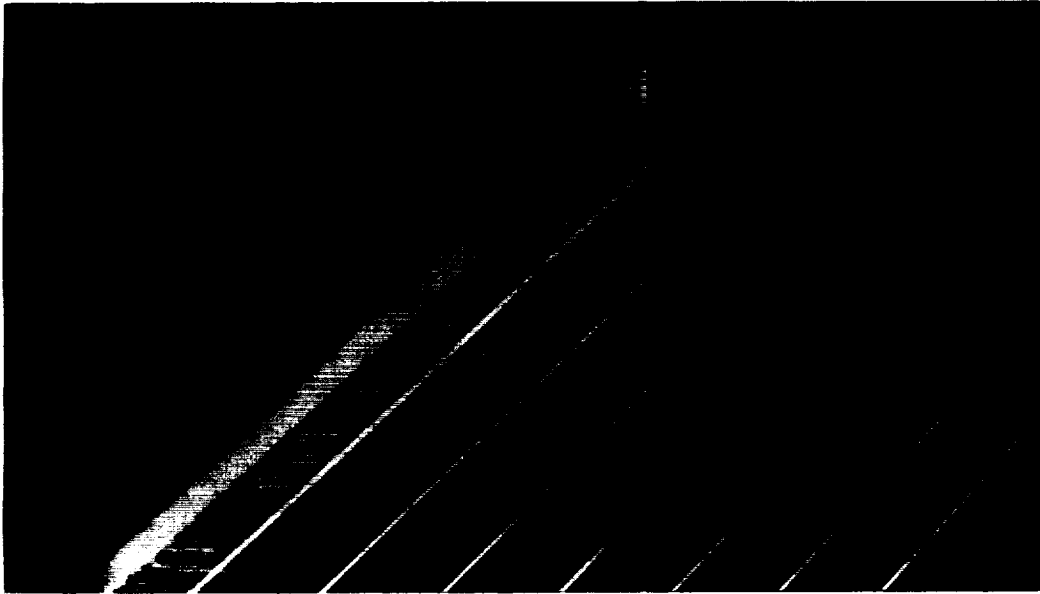
50
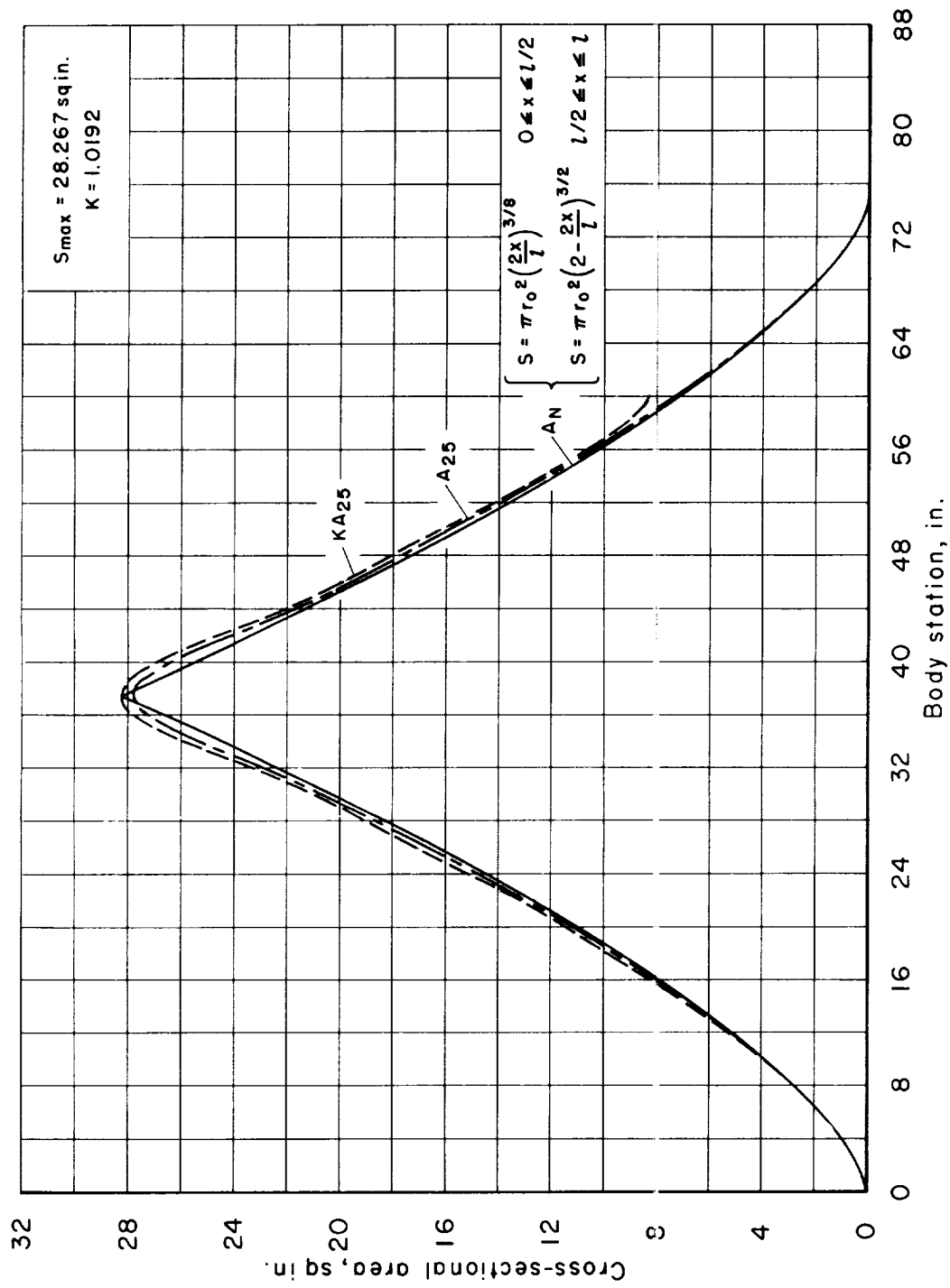


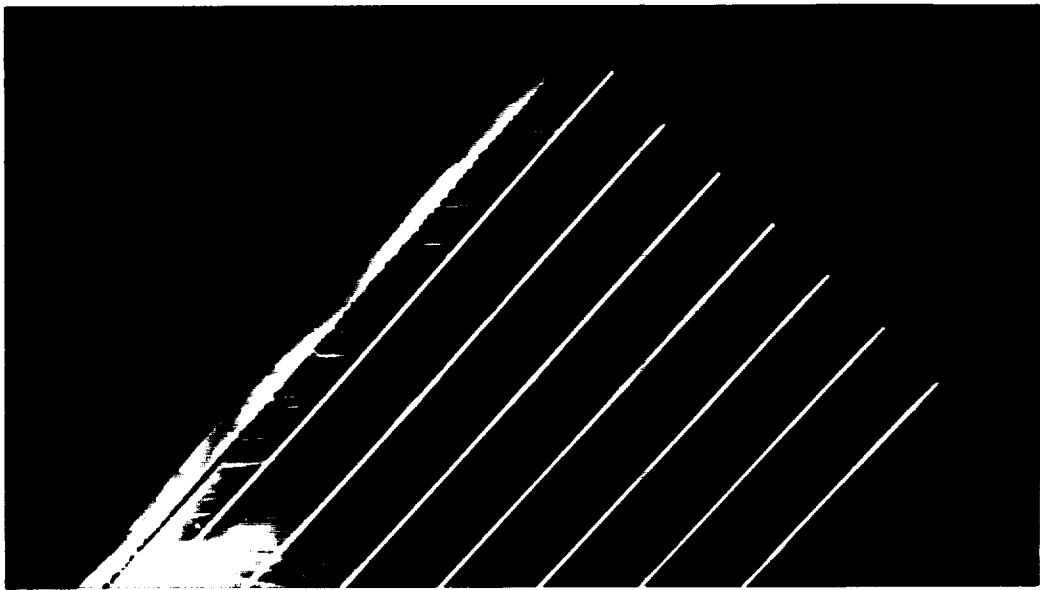Figure 16.— Derivation of the design area distribution, $KA_{25}$.
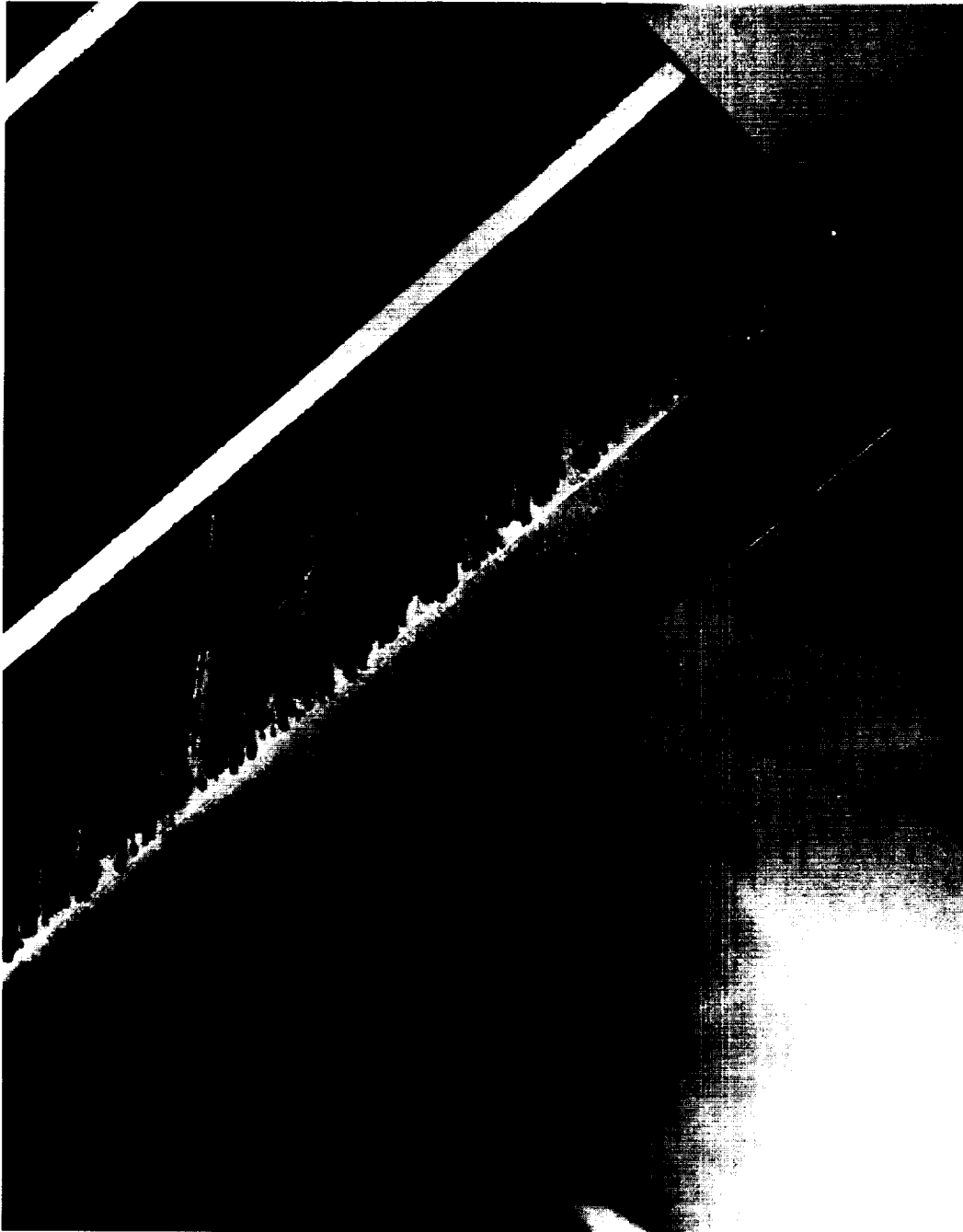
A-23660

Figure 17.- Full-scale photograph of the 0.040 inch grit used to fix transition on the diamond wing (preliminary test at M = 3.0 and R/ft = 3,000,000).

(a) M = 3.5, R/ft = 1,000,000, k = 0.060 inch



A-23675.1

(b) M = 3.5, R/ft = 3,000,000, k = 0.040 inch

Figure 18.- Conditions for which the fluorene sublimation material indicated unsatisfactory and satisfactory fixing of the boundary-layer transition.
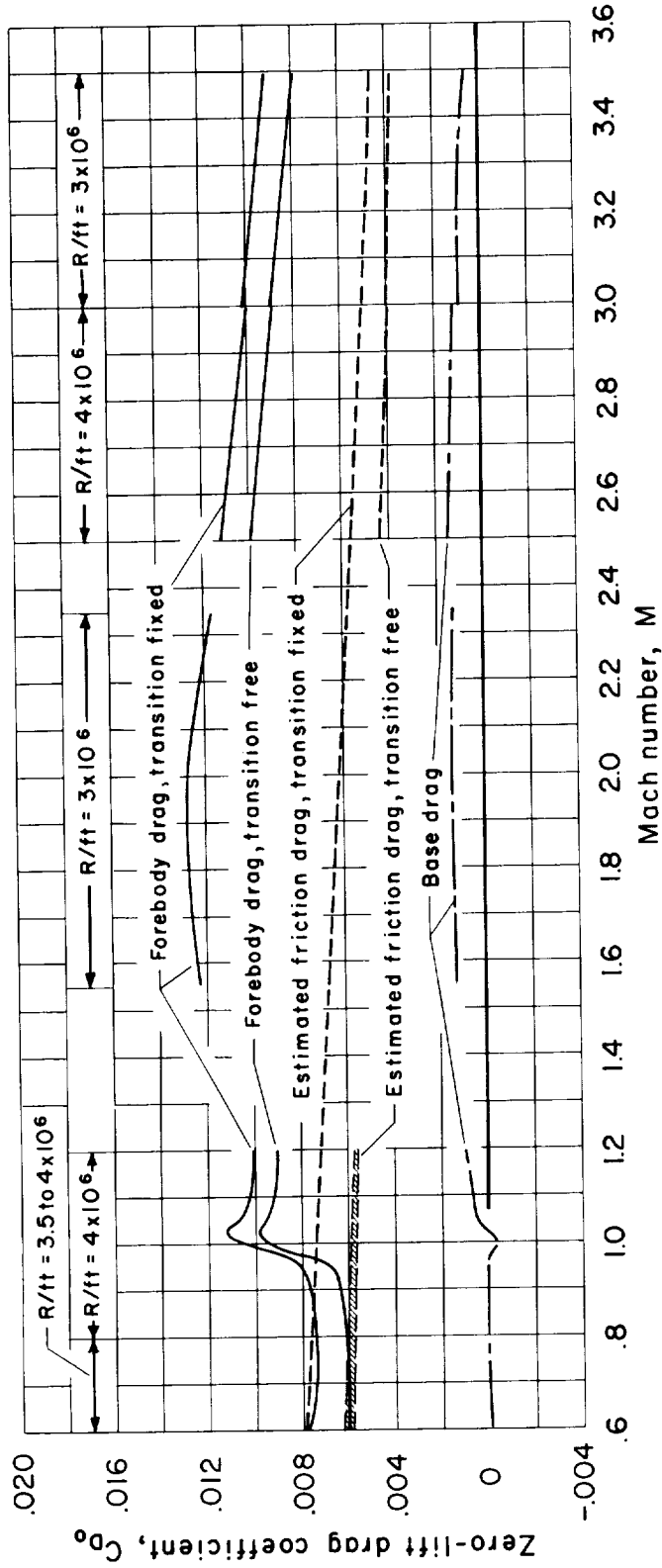
Figure 19.- Zero-lift drag coefficients for the diamond model with transition fixed and free.
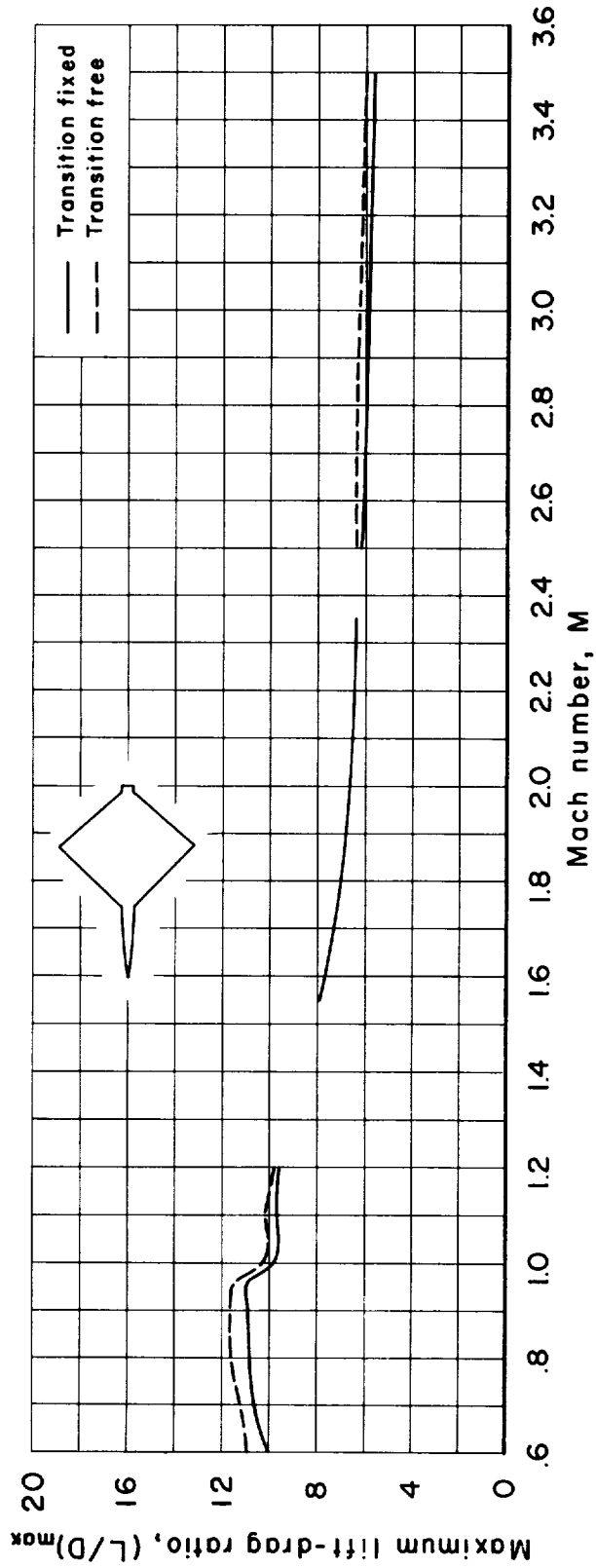
Figure 20.- Maximum lift-drag ratios for the diamond model with transition fixed and free.